Optimal operation of a system of charging hubs and a fleet of shared autonomous electric vehicles

Kevin A. Melendez*, Tapas K. Das, and Changhyun Kwon

Department of Industrial and Management Systems Engineering, University of South Florida

August 22, 2020

Abstract

Shared autonomous electric vehicles (SAEVs) are expected to serve a significant fraction of the passenger transportation needs in cities and surrounding urban areas. In this paper, we consider optimal operation of a cyber-physical system (CPS) comprising a large fleet of SAEVs and a set of charging hubs located across the transportation network and supported by the power grid. The hubs are considered to have a number of charging stations, a stand-alone battery bank for energy storage, and limited rooftop photo-voltaic (PV) generation capacity. We developed a robust mixed integer linear programming model. It considers a number of practical features of both the power and transportation systems, including day-ahead load commitment for electricity via an alternative current power flow model, real time price spikes of electricity, energy arbitrage, uncertainty in passenger demand, and balking of passengers while waiting for a ride. We demonstrated our methodology by implementing it on a sample CPS with 500 SAEVs and five hubs with fifty charging stations in each. Our methodology yields operational decisions for day ahead commitment of power and real time control of the SAEVs and the hubs. The sample CPS is used to examine impact of hub capacity and fleet size on various system performance measures. We discuss the computational challenges of our methodology and propose a simplified myopic approach that is capable of dealing with much larger fleet sizes and a variety of hub capacities. Reduction in computation time and the optimality gap for the myopic approach are examined.

Keywords— Shared autonomous electric vehicles, cyber-physical system, ACOPF, energy arbitrage, robust optimization, stochastic optimization

1 Introduction

Shared autonomous electric vehicles (SAEVs) are expected to replace a significant portion of the human driven automobiles on urban roads. The ride sharing companies serving cities and surrounding suburbs are

*Corresponding Author: kmelendez7@mail.usf.edu

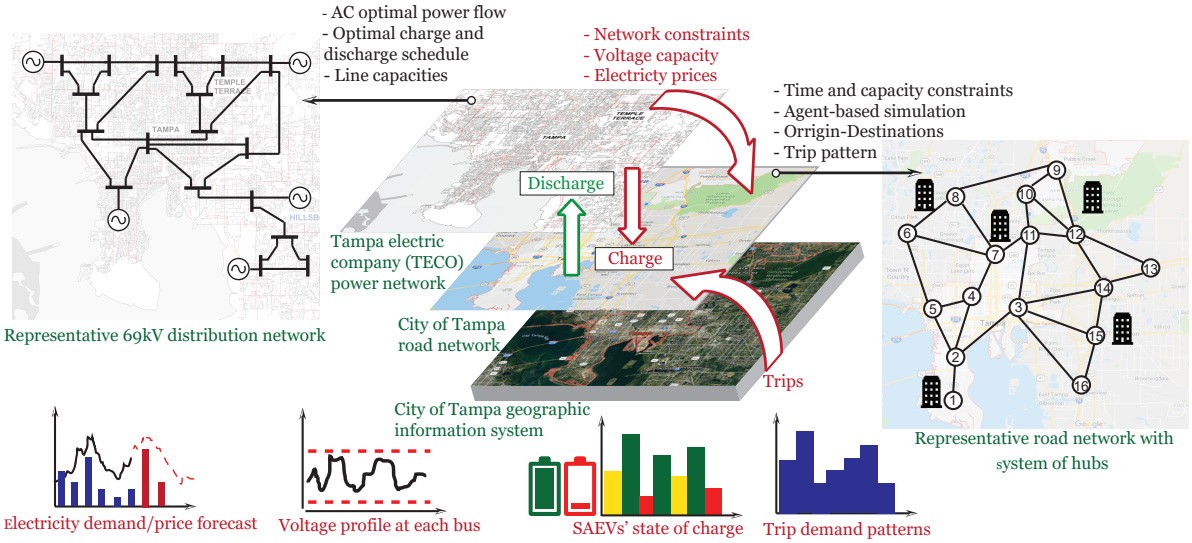

Figure 1: A three-tier diagram depicting interactions between population demographics, road network, and the power network in City of Tampa, Florida, USA

soon likely to adopt a new business model, which will use SAEVs leased from large feet-owning companies instead of cars owned and driven by individual contractors. However, switching to a fleet of SAEVs for ride sharing will be feasible only if a proper cyber-physical system (CPS) is available for charging the batteries as well as optimally coordinating the vehicles and the transportation needs. The CPS will comprise physical hubs with charging stations, located across the service area, together with a supervisory communication and control system that will optimally manage the real-time (RT) operation of the SAEVs and the hubs. The hubs may have limited solar (PV) generation and stand alone battery banks for energy storage. In addition to charging, the hubs are also capable of discharging both the SAEV batteries and the battery banks to sell power back to the grid, when appropriate (e.g., when the RT price of electricity is relatively high). The hubs may allow privately owned electric vehicle (EV) to charge for a fee when some charging stations are not occupied by the SAEVs. The control actions of the CPS includes making day ahead (DA) power purchase commitment for each hub and making real time operating decisions. The real time decisions will include 1) choosing the next action for each SAEV from among: serve a customer, charge or discharge at a hub, and idle at a parking lot, 2) for battery banks at each hub: either charge using grid/PV power or discharge to SAEVs and/or back to the grid, and 3) select the number of privately owned EVs to allow charging at each hub. Figure 1 presents a schematic of the 3-tiers of infrastructure (geographic distribution of the population centers, the transportation network, and the power network) that interacts with the CPS.

In this paper, we develop a methodology to maximize the gross profit of a CPS for varying transportation demand and electricity prices. We used daily operational cash flow (OCF) to calculate the gross profit; OCF includes fare received from the passengers, receipts from selling power back to the grid, charging fees from private EV owners, payment to the grid for electricity consumed, and parking fees paid for idling SAEVs. We did not consider the long term capital investment cost for physical facilities including charging hubs, vehicles, and maintenance facilities. We also did not consider the cost of human resources. We consider that the operational decisions for the fleet and the hubs are made in two stages by a central operator as follows. In the first stage, a commitment is made in the day ahead market for a fraction of the estimated hourly charging load, considering that any shortfall (or excess) can be bought (or sold) in the real time market. In the second

stage, real time operational decisions are made. The methodology thus has two stages. The first stage has three steps, which solves for the DA electricity commitment decisions as follows. In step 1, historical data for transportation demand, electricity prices, EV charging demand, and solar radiation are used to estimate the optimal demand consumption pattern of the CPS. In step 2, for each of these demand patterns, we solve an alternative optimal power flow (ACOPF) model and estimate the locational marginal prices (LMPs) and the corresponding real time (RT) prices. In step 3, the load patterns, the LMPs, and the RT prices are used to obtain a DA commitment using a stochastic model. The second stage of our methodology is formulated as a robust mixed integer linear program, solution of which decides the optimal actions for the SAEVs and the hubs in real time.

The application of the methodology on a sample CPS yields insights for how to design such a system. For example, determining the number of SAEVs, the number of the hubs and their capacities, selecting charging technology, sizing PV and battery banks, and decisions to allow charging of privately owned EVs. Our methodology considers a number of practical features of power markets and the transportation sector including two-time (DA and RT) power market settlement, prices spikes in the RT market, power network constraints via ACOPF model, time varying travel demands, and balking of passengers. Our methodology also addresses uncertainties in the RT electricity prices, PV generation, charging demands of privately owned EVs, and travel demand for the fleet vehicles. The use of our methodology will require data on historical electricity prices, transportation demand, solar generation, and EV charging demand. Data availability will depend on the part of the world our methodology is implemented. Electricity prices are generally publicly available in places where power market is deregulated, which is the case in some states in the U.S. and Canada, most countries in Europe, parts of Australia, New Zealand, among others. Similarly, public transportation data is also easily accessible as it is collected and curated by governmental institutions. Furthermore, private companies like Uber now share datasets with the public. Solar generation is also not difficult to estimate as solar irradiance data for areas/countries are generally available (see for U.S. https://www.energy.gov/maps/solar-energy-potential). Also, it is easy to use simple instruments like pyranometers to measure solar irradiance in an area of interest. As far as EV charging demand is concerned, it can be estimated from the demand in existing charging facilities in the area and the projected growth of EVs.

1.1 Contributions of this paper

Our methodology benefits from the original work done by Zhang et al. (2016) on autonomous vehicles scheduling and routing and the subsequent extension by Iacobucci et al. (2019) to incorporate price of electricity. However, our paper differs from the previous literature in three significant ways. First, our paper integrates the role of power networks in real time operational control of a fleet of SAEVs. We consider within the transportation model a number of power network related constraints, which have not been done in the open literature; most of the literature on electric vehicle integration focuses either mainly on the transportation aspects with simplifying assumptions about the electric power issues or vice versa. Our methodology considers both day-ahead and real time power markets and resulting price variations in making optimal fleet control decisions. We demonstrate the benefits of considering the power market in the operational decision making. The second novelty of our methodology is a reformulation of the transportation model presented in Zhang et al. (2016) and Iacobucci et al. (2019) for SAEV scheduling and routing. The model used in the above papers requires a significant number of integer variables, which makes the model computationally harder to solve. We proposed a reformulation of their model that reduces the number of integer variables. This allows us to solve the problem for relatively larger fleet sizes. The third distinction of our paper is the inclusion of a heuristic (myopic) model that finds reasonably good quality solutions with a significantly

reduced computation time.

Our methodology will create a number of other opportunities to benefit the electric power systems. As vehicle electrification soars, the percentage of electricity consumed for transportation will rise dramatically. A sizable part of this increase will be due to proliferation of SAEV-supported passenger ride sharing. Hence, a cyber-connected infrastructure for planned charging/discharging of large fleets of SAEVs will create an opportunity for network load balancing. Moreover, the temporal arbitrage potential of these fleets of vehicles would help power systems operators to reduce reserve generation requirement for maintaining system reliability. This is expected to reduce operational cost of the power networks and consequently reduce cost to all consumers.

The rest of the paper is organized as follows. Section 2 presents a brief review of the recent literature on EV and SAEV operations. In Section 3 we give an overview of the step by step approach of our methodology. Section 4 contains the models used in the two stages of our methodology. Section4.2 presents a planning model for SAEVs scheduling and charging. Ad hoc load schedule (obtained from the planning model) and market clearing price estimation are presented in Section 4.3. A two-stage stochastic model for day ahead commitment for the hubs is presented in Section 4.4. The real time operational model (for the second stage of our methodology) is given in Section 4.5. Our methodology is implemented on a case study built using demographic and transportation information from the City of Tampa and its suburbs (in the state of Florida in the U.S.). Since the city of Tampa is part of a regulated power network, we adopted information concerning electric power from a deregulated network in the U.S. (PJM). Results from the case study are presented in Section 5. Due to the computational complexities of some of the steps of our methodology, an alternative myopic modeling approach is given in section 6 and its performance is examined in Section 7. Section 8 contains the concluding remarks.

2 Related literature

Although there is abundant literature on charging infrastructure design for optimal operation of privately owned EVs, literature on SAEVs addressing issues like strategies for charge and discharge, locating charging stations, and algorithms for real-time control are still very limited (Iacobucci et al. 2019). Our study of the literature reveals that almost all of the relevant models for operation of EV or SAEV focus primarily on either the transportation or the electricity aspects of the problem. For example, charging-facility (hub) sizing and location models are typically approached from the transportation perspective. Whereas most of the models for optimal operation of EVs and charging facilities consider power related constraints and uncertainties. Hub sizing and location models consider temporal-spatial distribution of the origin-destination of the trips, charging stations availability across the road network, and charging strategies with implicit assumption that the power network related constraints are satisfied. On the other hand, the operational models are formed using electricity network characteristics, such as varying electricity prices, arbitrage contracts, active and reactive power, voltage capacities, and other network constraints, while considering the transportation related parameters as exogenous. Since the primary focus of our paper is on optimal operations of SAEVs and charging hubs, most of our literature review discusses papers addressing operational aspects. We first cover the literature that deal with privately owned EVs and thereafter we focus on SAEVs.

Optimal operation of EV fleets has received much attention in the recent literature. Operation of parking/charging lots for EVs at workplaces and commercial buildings is examined in Sedighizadeh et al. (2019). The paper considers making power purchase commitments in the day ahead market and uncertainties in the demand for charging, EV arrival and departure times, and electricity prices. However, some of the

common features like providing load balancing to the grid and use of renewable generation for charging of the EVs by are not included. A real-time charging scheme for EV parking lots, enabling them to participate in demand response programs, is studied via a deterministic model in Yao et al. (2017). The model manages the impact of parking lots on the power grid by setting a maximum limit to the power that can be drawn at any point in time. It considers the charging priorities of all connected EVs to satisfy energy requirements while also guarantying fairness. The authors in Subramanian & Das (2019) present a model to study how increasing demand response capacity of a growing number of EV parking lots will promote dynamic pricing of electricity. The model considers day-ahead and real-time settlements, power network constraints (including congestion), real time prices uncertainties, a granular operational model for the parking lot, and EVs with different battery capacities and charging needs. However, injecting power back to the grid or any other forms of temporal arbitrage are not considered. A model offered in Turan et al. (2019) minimizes power consumption of an EV parking lot that is supplied by both the grid as well as rooftop photo-voltaic panels. The model features include charging from non-dispatchable generation, dynamically varying electricity prices, and reserve power for grid support. The authors in Melendez et al. (2019) use a coalition of connected EVs for peer-to-peer trading. It was found that peers participating in the sample network can reduce their total cost between 14.17% and 22.7%, while maintaining fairness.

Several papers on the operation of SAEV fleets and location of charging hubs have recently appeared in the open literature. A model proposed in Lam et al. (2018) studies how to coordinate a fleet of autonomous EVs to park at appropriate parking facilities to support vehicle-to-grid services. The model does not consider the electricity price and assumes that the location of all vehicles is known in advance. The authors develop a distributed algorithm based on dual decomposition to solve the model efficiently. A fleet of SAEVs is simulated in Chen et al. (2016) via a discrete-time agent-based model. It examines the capabilities of these vehicles to be shared and self-charged while considering passenger travels needs. The results from the simulation model are used to analyze the impacts of vehicle range and charging infrastructure on the fleet size, charging station location, ability to meet trip demand, user wait times, and induced vehicle-miles traveled. The above agent-based simulation model was extended in Farhan & Chen (2018). The extended model determines the optimal routes to pick up and drop off multiple travelers within a given time interval using vehicles with fixed seating capacities. The problem is formulated as a capacitated vehicle routing problem with time windows, which is then decomposed into a number of subproblems. The solution methodology first assigns travel requests to vehicles and then constructs an itinerary for pick up and drop off. Farhan & Chen (2018) claims their study to be the first to analyze the dynamic ridesharing operations of SAEVs from the perspective of a fleet operator. A two-stage multi-objective optimization model for planning of an autonomous connected electric vehicle (ACEV)-based car-sharing system is given in Miao et al. (2019). Each stage is a multi-objective optimization model where both users and service providers objectives are considered. The authors also propose a hybrid parking mechanism to attain a compromise between user flexibility and system management efficiency. The work presented in Kang et al. (2017) offers a framework to optimally design a fleet of autonomous electric vehicles. The framework comprises four components, namely, fleet size and assignment schedule, sizing and location of charging stations, vehicle powertrain requirements, and service fees.

A methodology to simultaneously optimize SAEV charging, routing, and rebalancing can be found in Iacobucci et al. (2018*a*). It considers two different time scales for solving the transportation and charging problems for a fleet of SAEVs, by using a model-predictive control approach. The charging of the vehicles is optimized over longer time scales to minimize electricity costs. The results from the charging optimization problem are used as constraints for the vehicle routing and rebalancing problem, which is optimized at shorter

time-scales. The objective function for the methodology is formulated as the weighted sum of the passenger waiting time, rebalancing time, and the cost of electricity; the cost of electricity is assumed to be known. The methodology in Iacobucci et al. (2018*a*) was extended in Iacobucci et al. (2019) to consider injecting power back to the grid (V2G). According to the authors, optimal rebalancing of SAEVs and their charging with time-varying electricity prices have not been presented to the literature earlier. The work in Iacobucci et al. (2018*b*) presentess a mixed-integer linear program to optimally schedule charge and discharge of an aggregation of SAEVs to minimize total operational costs of microgrids or virtual power plants.

Our methodology for optimal joint operation of a system of hubs and a large fleet of SAEVs differs from the literature discussed above in a number of significant ways. Instead of assuming time varying prices of electricity to be known, we incorporate power network operations in our methodology by embedding an ACOPF model. The ACOPF model yields the day ahead market clearing prices (MCPs) considering power consumption by the base load (of the community) as well as the loads generated by the SAEVs. The loads from SAEVs are determined by the vehicle scheduling and charging strategies. We model the RT prices of electricity at the network nodes by using the MCPs and estimates of the frequency and amplitude of price spikes. We use the DA and estimated RT prices to make the DA commitments for the hubs, which are then used to solve a real time model for making operational decisions for the SAEVs (i.e., to serve a demand, to charge, to discharge, or to park and idle). The hubs are assumed to have limited solar generation and battery storage capacities.

3 Overview of the Operational Methodology

In this section, we present a brief outline our methodology. Stage 1 obtains the DA commitment for each hub and stage 2 obtains real time operational strategies.

- **Stage 1: Obtaining DA commitment for each hub**
  - **Step 1.** *Develop ad hoc load schedule scenarios*: For this step, we first gather a large number of (daily) historical data sets on prices of electricity, transportation demand for SAEVs, amount of PV generation at the hubs, and charging demand for privately owned EVs. For each daily data scenario, we solve a planning model (given in subsection 4.2) to obtain an operational strategy for the SAEVs and the hubs that maximizes the gross profit. The gross profit includes: fare received from the passengers, receipts from selling power back to the grid, charging fees from the private EV owners, payment to the grid for electricity consumed, and parking fees paid for idling SAEVs. The planning model yields, for each daily data scenario, a load consumption schedule for each hub. A scenario reduction technique, available in Growe-Kuska et al. (2003), is then used to select a small subset of the load schedules at the hubs. As alluded earlier, the system operational strategy obtained by the planning model comprises decisions on 1) choosing the next action for each SAEV, namely, whether to serve a customer, charge or discharge at a hub, or idle at a parking lot, 2) operating the battery banks at each hub to either charge or discharge, and 3) selecting the number of privately owned EVs to allow charging at each hub.
  - **Step 2.** *Calculate DA MCPs and RT prices*: For each of the selected load schedule scenarios from step 1, together with the existing base loads at the nodes of the power grid to which hubs are connected, we solve an ACOPF model. The ACOPF yields the DA MCPs at each node. Using an existing approach from the literature (Das & Wollenberg 2005), we use these MCPs to generate daily RT prices with spikes.

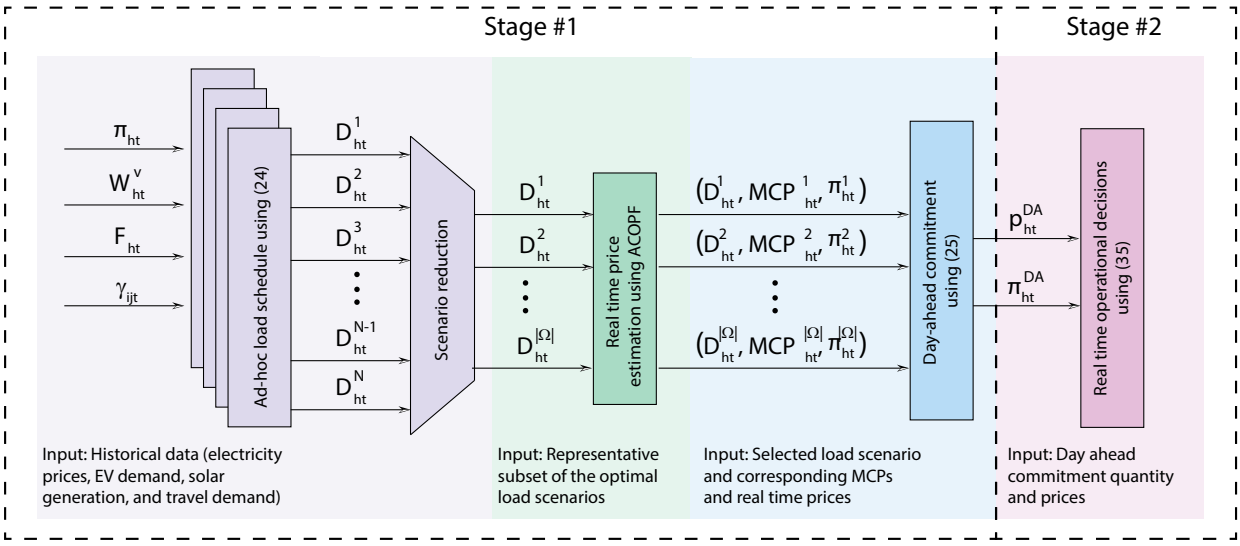

Figure 2: Summary of the operational methodology

  - **Step 3.** *Obtain DA commitment for each hub*: In this step, for each load schedule from Step 1 and corresponding MCP and estimated RT prices from Step 2, we determine the DA commitment for each time interval for each hub. To obtain the DA commitment, we use a two stage stochastic model in order to minimize the total expected cost of power purchase by optimally balancing the purchases from the DA and the RT markets. The two stage model considers the variations in MCPs and RT prices over all time intervals of a day.

- **Stage 2: Develop a real time operational strategy for the CPS**: In this stage of our methodology, we use a robust version the planning model to accommodate the uncertainties associated with parameters such as transportation demand, RT prices, PV generation at the hubs, and EV charging demand. Instead of assuming the uncertain parameters to be known for all time period of the day, as in the planning model, the real time model assumes that parameters values of the current time period only are known and considers confidence intervals for the remaining time periods of the day.

Schematic of the complete methodology is presented in Figure 2. The main input parameters (electricity prices, EV demand, solar generation, and travel demand) to the methodology are the sources of uncertainty for the model (24). In the first step of our methodology, we solve many instances of the model (24) for different combinations of values of these parameters in order to obtain estimated amounts of load consumed by the system across the hours of the day (adhoc load schedules). These adhoc schedules will drive the decision for the rest of the steps. It may be noted that electricity price is the only parameter used explicitly in equation (24). The other parameters (EV demand, solar generation, and travel demand) are part of the constrains of the model.

4 Operational Methodology

In this section, we present the models used in our methodology.

4.1 Notation

For ease of reference, below find the complete notation used in our methodology.

Sets

- $\mathcal{B}$: Set of all SAEVs
- $\overline{\mathcal{T}}$: Set of all time periods
- $\overline{\mathcal{N}}$: Set of all nodes on the transportation network
- $\mathcal{A}$: Set of all arcs in the transportation network
- $\mathcal{H}$: Subset of transportation nodes where hubs are located
- $\mathcal{P}$: Subset of transportation nodes with parking/idling facilities
- $\mathcal{D}_h$: Set of minimum cost load schedules at hub h
- Ω: Subset of selected scenarios (load, MCP, and RT price) across all hubs

Parameters

- γ_{ijt}: Number of passenger arrivals at node i with destination j $(i,j) \in \mathcal{A}$ at time $t \in \overline{\mathcal{T}}$
- τ_{ij}: Travel time between nodes i and j $(i,j) \in \mathcal{A}$
- β: Balking rate $(0 \leq \beta \leq 1)$ of waiting passengers
- α_p: Parking fee per each time period at parking lot $p \in \mathcal{P}$
- ψ_t: Price paid by the customer per each time period for a trip originating at time $t \in \overline{\mathcal{T}}$
- ζ_h: Facility fee paid by privately owned EVs per each time period when charging at hub $h \in \mathcal{H}$
- π_{ht}: Historical price of electricity at the node supporting hub $h \in \mathcal{H}$ at time $t \in \overline{\mathcal{T}}$
- π_{ht}^{DA}: Published DA price at node $h \in \mathcal{H}$ at time $t \in \overline{\mathcal{T}}$
- π_{ht}^{RT}: Actual RT price at node $h \in \mathcal{H}$ at time $t \in \overline{\mathcal{T}}$
- π_{ht}^{ω}: Estimated RT price in scenario $\omega \in \Omega$ at hub $h \in \mathcal{H}$ at time period $t \in \overline{\mathcal{T}}$
- ϕ_b: Battery capacity of SAEV $b \in \mathcal{B}$
- ϵ_b: Energy consumption of SAEV $b \in \mathcal{B}$ per each time period on the road
- $\underline{S_b}, \overline{S_b}$: Lower and upper bounds of state of charge for SAEV $b \in \mathcal{B}$
- $\overline{P}^{+}$: Maximum energy that can be added to a vehicle per time period, same for all hubs
- $\overline{P}^{-}$: Maximum energy that can be discharged from a vehicle per time period, same for all hubs
- F_{ht},$F_h^{\max}$: Solar generation at hub $h \in \mathcal{H}$ at time $t \in \overline{\mathcal{T}}$ and installed solar capacity, respectively
- E_h,$\overline{P}_h$,$\underline{P}_h$: Capacity, charging rate, and discharging rate, respectively, of the battery bank at hub $h \in \mathcal{H}$
- V: Maximum number of time periods that a privately owned EV can charge in a hub

- W_{ht}^{v}: Number of privately owned EVs requesting charging services for $v \leq V$ time periods at hub $h \in \mathcal{H}$ at time $t \in \overline{\mathcal{T}}$
- C_h: Total number of charging stations installed at hub $h \in \mathcal{H}$
- D_{ht}: Minimal cost load schedule for each time period $t \in \overline{\mathcal{T}}$ at hub $h \in \mathcal{H}$ ($D_{ht} \in \mathcal{D}_h$)
- D_{ht}^{ω}: Selected load schedule for each time period $t \in \overline{\mathcal{T}}$ at hub $h \in \mathcal{H}$ from scenario $\omega \in \Omega$
- μ^{ω}: Probability of scenario $w \in \Omega$
- P_{ht}^{DA}: DA commitment of hub $h \in \mathcal{H}$ at time period $t \in \overline{\mathcal{T}}$

Decision variables

- x_{ijt}^{b}: 1 if vehicle $b \in \mathcal{B}$ is departing with passengers from node i to node j at time $t \in \overline{\mathcal{T}}$, and 0 otherwise
- y_{ijt}^{b}: 1 if vehicle $b \in \mathcal{B}$ is departing empty from node i to node j at time $t \in \overline{\mathcal{T}}$, and 0 otherwise
- p_{ht}^{b+}: Total charge added to SAEV $b \in \mathcal{B}$ at hub $h \in \mathcal{H}$ at time period $t \in \overline{\mathcal{T}}$
- p_{ht}^{b-},p_{ht}^{-}: Total energy discharged from SAEV $b \in \mathcal{B}$ and from the battery bank, respectively, at hub $h \in \mathcal{H}$ and time period $t \in \overline{\mathcal{T}}$
- $\hat{p}_{ht}^{-}$: Fraction of the total discharged energy sold to the main grid by the battery bank at hub $h \in \mathcal{H}$ and time period $t \in \overline{\mathcal{T}}$
- e_{ht}^{b},e_{ht}^{EV}: Energy added form the battery bank to SAEV $b \in \mathcal{B}$ and privately owned EVs, respectively, at hub $h \in \mathcal{H}$ at time period $t \in \overline{\mathcal{T}}$
- f_{ht}^{b},f_{ht}^{+},f_{ht}^{EV}: Solar energy added to SAEV $b \in \mathcal{B}$, battery bank, and privately owned EVs, respectively, at hub $h \in \mathcal{H}$ and time period $t \in \overline{\mathcal{T}}$
- f_{ht}^{-}: Solar energy dispatched directly to the main grid
- g_{ht}^{b},g_{ht},g_{ht}^{EV}: Total energy bought from the grid to charge SAEV $b \in \mathcal{B}$, the battery bank, and the privately owned EVs, respectively, at hub $h \in \mathcal{H}$ and time period $t \in \overline{\mathcal{T}}$
- w_{ht}^{b+}: 1 if SAEV $b \in \mathcal{B}$ is charging at hub $h \in \mathcal{H}$ and time period $t \in \overline{\mathcal{T}}$, 0 otherwise
- w_{ht}^{b-}: 1 if SAEV $b \in \mathcal{B}$ is discharging at hub $h \in \mathcal{H}$ and time period $t \in \overline{\mathcal{T}}$, 0 otherwise
- $p_{ht}^{\mathrm{RT}-}$: Fraction of the DA commitment sold to the RT market by hub $h \in \mathcal{H}$ at time period $t \in \overline{\mathcal{T}}$
- w_{ht}^{v}: Number of charging stations assigned to privately owned EVs at hub $h \in \mathcal{H}$ at time period $t \in \overline{\mathcal{T}}$; the vehicles stay v time periods at the hubs

Other variables

- z_{it}^{b}: 1 if vehicle $b \in \mathcal{B}$ waited in node $i \in \overline{\mathcal{N}}$ from time $t-1$ to t, and 0 otherwise
- p_{it}^{b}: 1 if at time period $t \in \overline{\mathcal{T}}$, the vehicle $b \in \mathcal{B}$ will arrive at node $i \in \overline{\mathcal{N}}$
- d_{ijt}: Number of passengers left unserved at node i with destination j ($i, j \in \overline{\mathcal{N}}$) at time period $t \in \overline{\mathcal{T}}$
- b_{ijt}: Dummy variable to avoid infeasibility ($0 \leq b_{ijt} \leq 1$)
- s_{t}^{b},s_{ht}: State of charge of SAEV $b \in \mathcal{B}$ and the battery bank in hub $h \in \mathcal{H}$, respectively, at time period $t \in \overline{\mathcal{T}}$; $0 < s_{t}^{b} < 1$,$0 < s_{ht} < 1$, $\forall b, h, t$

- a^{RT}: RT electricity profit, i.e., revenue from selling to the grid in the RT market minus cost of buying in the RT market
- c_{ht}: Number of charging stations occupied by privately owned EVs at hub $h \in \mathcal{H}$ at time period $t \in \overline{\mathcal{T}}$

4.2 Planning Model for Ad-Hoc Load Schedules

The planning model is formulated as a mixed integer program with the objective of maximizing the gross profit from the operation of the CPS. The operational elements considered in the model are: serving the transportation needs, charging and discharging of the SAEVs and the battery banks, utilization of the PV generation, and acceptance of EV charging requests. In what follows, we first develop all the necessary constraints related with transportation (1)–(6), energy (7)–(19), and privately owned EVs (20)-(23). Thereafter, we present the complete of the planning model in (24).

The transportation model formulation that we have considered is inspired by the model proposed in Zhang et al. (2016) for vehicle scheduling and routing in autonomous mobility-on-demand systems. The model in Zhang et al. (2016) was expanded to consider charging constraints and V2G in Iacobucci et al. (2018*a*) and Iacobucci et al. (2019), respectively. The model formulations in these papers keep track of the vehicles' positions while traveling within an arc of the transportation network, which significantly increases the complexity of the models. We develop a simplified version of the model presented in Zhang et al. (2016), that uses a significantly less number of binary variables, and extend it to consider balking of the passengers and power-market-related constraints as follows.

Let $\overline{\mathcal{T}}$ be the set of all time periods, $\overline{\mathcal{N}}$ be the set of all nodes in the transportation network, and $\mathcal{A}$ be the set of all i, j combinations in the network. We define γ_{ijt} and d_{ijt} as the number of new passenger demand arrivals and the unserved demand, respectively, at node i with destination j, $(i,j) \in \mathcal{A}$, at time $t \in \overline{\mathcal{T}}$. Let $\mathcal{B}$ denote the set of all SAEVs. We define, for $b \in \mathcal{B}$, $x^b_{ijt} = 1$ if vehicle b departs with a passenger from node i to node j at time period t, and 0 otherwise. The demand left unserved in any given node is equal to the number of customers already waiting, plus the new arrivals, minus the demand served at the current time:

$$d_{ij,t+1} = (1-\beta)d_{ijt} + \gamma_{ijt} - \sum_{b\in\mathcal{B}} x^b_{ijt} - b_{ijt}, \qquad \forall (i,j) \in \mathcal{A}, t \in \overline{\mathcal{T}}, \tag{1}$$

where $\beta \in (0,1)$ denotes the fraction of the already waiting customers that balk. A the dummy variable b_{ijt} $(0 \le b_{ijt} \le 1)$ is introduced to cancel out the fractional part of $(1-\beta)d_{ijt}$ and ensure that $d_{ij,t+1}$ is integer. Let $\mathcal{H}$ and $\mathcal{P}$ be the subsets of the nodes in the transportation network in which the smart hubs and parking facilities are located, respectively. We define $z^b_{it} = 1$, if vehicle b waited in node i from time $t-1$ to time t, and 0 otherwise. Then, the following constraint guarantees that SAEVs park only at nodes with parking lots or smart hubs.

$$z^b_{it} = 0, \qquad \forall t \in \overline{\mathcal{T}}, b \in \mathcal{B}, i \notin \mathcal{H} \cup \mathcal{P}. \tag{2}$$

Let $y^b_{ijt} = 1$, if vehicle b is departing empty from node i to j at time period t, and 0 otherwise. Also let $p^b_{it} = 1$, if at time t, the vehicle b arrives at node i. Then, the following constraints determine if vehicle b stays at, arrive to, or depart from node i at time t.

An SAEV arrives to node i at time t if it departed from node j exactly τ_{ji} time periods before, where τ_{ji}

is the travel time between nodes j and i. Then, we can write that

$$p_{it}^b = \sum_{(j,i)\in\mathcal{A}:\tau_{ji}\leq t} (x_{ji,t-\tau_{ji}}^b + y_{ji,t-\tau_{ji}}^b), \qquad \forall i \in \overline{\mathcal{N}}, t \in \overline{\mathcal{T}}, b \in \mathcal{B}. \tag{3}$$

Constraint (4) ensures that the vehicle will either stay parked at a node or depart from it with or without passenger; none of these actions can occur simultaneously.

$$\sum_{i\in\overline{\mathcal{N}}} (z_{i,t+1}^b + \sum_{(i,j)\in\mathcal{A}} x_{ijt}^b + \sum_{(i,j)\in\mathcal{A}} y_{ijt}^b) \leq 1, \qquad \forall t \in \mathcal{T}, b \in \mathcal{B}. \tag{4}$$

The next constraint, assures that if a vehicle is at a node, it must have either just arrived or been idling since the previous time period.

$$z_{it}^b + p_{it}^b \leq 1, \qquad \forall i \in \overline{\mathcal{N}}, t \in \overline{\mathcal{T}}, b \in \mathcal{B}. \tag{5}$$

An SAEV stays at a node for the next time period if it was already idling at a node and did not depart in the current time period. This considered in the following constraint.

$$z_{i,t+1}^b = z_{it}^b + p_{it}^b - \sum_{(i,j)\in\mathcal{A}} (x_{ijt}^b + y_{ijt}^b), \qquad \forall i \in \overline{\mathcal{N}}, t \in \overline{\mathcal{T}}, b \in \mathcal{B}. \tag{6}$$

In the remaining part of this subsection, we model the vehicle charging aspect of the problem. Charging schedule of the SAEVs depends on the varying electricity prices at the nodes and the transportation demand. The smart hubs are considered to offer charging services to privately owned EVs. The fleet operator may charge SAEVs when the prices are low and sell the excess energy to the grid if the prices are high enough. The DA commitment of the hubs may also be sold back to the grid if the RT prices rise significantly. Finally, we consider that each hub also has a bank of stand-alone batteries and rooftop solar generation, which give additional flexibility to the CPS operator. The fleet of SAEVs is subject to routing constraints (1)–(6) as well as some charging constraints as follows.

Let ϕ_b denote the battery capacity of SAEV b, ϵ^b be the energy consumed by SAEV b per unit time period on the road, p_{ht}^{b+} be the total charge added to SAEV b at hub h at time period t, and p_{ht}^{b-} be total energy discharged from SAEV b at hub h and time period t. The state of charge of SAEV b, denoted by s_t^b, changes over time depending on whether the vehicle is charging, discharging, idling or traveling. Then, we can write the energy conservation of SAEV b as

$$\phi_b s_{t+1}^b = \phi_b s_t^b + \sum_{h\in\mathcal{H}} p_{ht}^{b+} - \sum_{h\in\mathcal{H}} p_{ht}^{b-} - \epsilon^b \left(1 - \sum_{i\in\overline{\mathcal{N}}} z_{i,t+1}^b\right), \qquad \forall t \in \overline{\mathcal{T}}, b \in \mathcal{B}. \tag{7}$$

Note from (7) that if SAEV b has been parked at any node i (i.e., $z_{i,t+1}^b = 1$), then the last term is equal to zero (no energy consumed for travel). Total energy charged to an SAEV b might come from either the grid (g_{ht}^b), the rooftop solar system (f_{ht}^b), or the bank of stand-alone batteries (e_{ht}^b). Then, we can write the total amount charged as

$$p_{ht}^{b+} = e_{ht}^b + f_{ht}^b + g_{ht}^b, \qquad \forall t \in \overline{\mathcal{T}}, b \in \mathcal{B}, h \in \mathcal{H}, \tag{8}$$

where

$$f_{ht}^{b} \leq F_{h}^{\max} z_{h,t+1}^{b}, \qquad \forall t \in \overline{\mathcal{T}}, b \in \mathcal{B}, h \in \mathcal{H}, \tag{9}$$

$$e_{ht}^{b} \leq E_{h} z_{h,t+1}^{b}, \qquad \forall t \in \overline{\mathcal{T}}, b \in \mathcal{B}, h \in \mathcal{H}, \tag{10}$$

and $F_h^{\max}$ is the installed capacity of solar power and E_h is the aggregated stand-alone battery capacity. Note that $F_h^{\max}$ and E_h are acting as big-Ms in these equations. We assume that both charge and discharge rates for the vehicles are constant and denoted by P^+ and P^-, respectively. Hence, we can write that

$$p_{ht}^{b+} \leq P^{+} w_{ht}^{b+}, \qquad \forall t \in \overline{\mathcal{T}}, b \in \mathcal{B}, h \in \mathcal{H}, \tag{11}$$

$$p_{ht}^{b-} \leq P^{-} w_{ht}^{b-}, \qquad \forall t \in \overline{\mathcal{T}}, b \in \mathcal{B}, h \in \mathcal{H}. \tag{12}$$

where w_{ht}^{b+} and w_{ht}^{b-} are binary variables equal to 1 if SAEV b is charging or discharging, respectively, at hub h at time period t, and 0 otherwise. The next constraint guarantees that 1) the SAEVs can charge or discharge only if they are parked at a hub and, 2) they are not charging and discharging simultaneously during time period t:

$$w_{ht}^{b+} + w_{ht}^{b-} \leq z_{h,t+1}^{b}, \qquad \forall t \in \overline{\mathcal{T}}, b \in \mathcal{B}, h \in \mathcal{H}. \tag{13}$$

We assume that the state of charge of SAEV batteries may not be allowed to be either 0 or 1. We define $\underline{S_b}$ and $\overline{S_b}$ as the minimum and maximum allowable state of charge for SAEV b at any time, respectively. Then SAEVs state of charge is bounded by

$$\underline{S^{b}} \leq s_{t}^{b} \leq \overline{S^{b}}, \qquad \forall t \in \overline{\mathcal{T}}, b \in \mathcal{B}. \tag{14}$$

Let P_h^+, and P_h^- be the charging and discharging rates, respectively, of the bank of stand alone batteries at hub h. Let g_{ht} and f_{ht}^+ be the fraction of the energy charged to the bank of stand-alone batteries coming from the grid and the available solar power, respectively. Let p_{ht}^- denote the total energy discharged from the bank of stand-alone batteries at hub h at time period t and s_{ht} (between 0 and 1) denote its state of charge. Then, power conservation of the bank of stand-alone batteries is given by:

$$E_h s_{h,t+1} = E_h s_{ht} + g_{ht} + f_{ht}^{+} - p_{ht}^{-}, \qquad \forall t \in \overline{\mathcal{T}}, h \in \mathcal{H}, \tag{15}$$

where both the charging and discharging rates of the battery bank are bounded as:

$$g_{ht} + f_{ht}^{+} \leq P_{h}^{+}, \qquad \forall t \in \overline{\mathcal{T}}, h \in \mathcal{H}, \tag{16}$$

$$p_{ht}^{-} \leq P_{h}^{-}, \qquad \forall t \in \overline{\mathcal{T}}, h \in \mathcal{H}. \tag{17}$$

Energy discharged from the bank of stand-alone batteries is used to 1) charge the SAEVs and the privately owned EVs at the hubs, and 2) to sell in the RT market (denoted by $\hat{p}_{ht}^-$). Hence, we can write that

$$p_{ht}^{-} = \sum_{b \in \mathcal{B}} e_{ht}^{b} + e_{ht}^{\mathrm{EV}} + \hat{p}_{ht}^{-}, \qquad \forall t \in \overline{\mathcal{T}}, h \in \mathcal{H}, \tag{18}$$

where, e_{ht}^{EV} is the total energy added form the bank of stand-alone batteries to the privately owned EVs at hub h at time period t. Similarly, the available solar power at the hubs (F_{ht}) is used to 1) charge the parked SAEVs, the bank of stand-alone batteries, and the privately owned EVs (f_{ht}^{EV}), and 2) to sell in the

RT market (f^-_{ht}). Then we have that:

$$\sum_{b\in\mathcal{B}} f^b_{ht} + f^{\text{EV}}_{ht} + f^+_{ht} + f^-_{ht} = F_{ht}, \qquad \forall t \in \overline{\mathcal{T}}, h \in \mathcal{H}. \tag{19}$$

When appropriate, the CPS operator discloses availability of charging stations in the hubs to privately owned EVs. The EV owners pay the RT price of electricity plus a fee ζ_h for each period they occupy a charging station at the hubs. Without loss of generality, we consider that EV oweners will request v number of time periods to the hubs; $v \in \{1, \cdots, V\}$, where V is the maximum number of time periods that a privately owned EV is allowed to stay (charging) at a hub. Let W^v_{ht} be the number of EVs requesting charging for v time periods at hub h at time period t, and w^v_{ht} is the number of requests that are accepted; note that W^v_{ht} is a parameter whereas w^v_{ht} is a decision variable. The EV charging requests that are accepted in the current time period will occupy charging stations at the hubs at the beginning of the next time period. Then, we have that:

$$w^v_{h,t+1} \leq W^v_{ht}, \qquad \forall h \in \mathcal{H}, t \in \overline{\mathcal{T}}. \tag{20}$$

The number of charging stations used by privately owned EVs at any time t (c_{ht}) is equal to the number of accepted request for time period t, plus, the number of EVs that were charging in the previous time periods. Then, we can right that

$$c_{ht} = \sum_{v=1}^{V} w^v_{ht} + \sum_{v=2}^{V} w^v_{h,t-(v-1)}, \qquad \forall h \in \mathcal{H}, t \in \overline{\mathcal{T}}. \tag{21}$$

As the total energy consumed by the privately owned EVs is supplied by the grid (g^{EV}_{ht}), the bank of stand-alone batteries (e^{EV}_{ht}), and solar power (f^{EV}_{ht}), we have that:

$$e^{\text{EV}}_{ht} + f^{\text{EV}}_{ht} + g^{\text{EV}}_{ht} = P^+ c_{ht}, \qquad \forall h \in \mathcal{H}, t \in \overline{\mathcal{T}}. \tag{22}$$

The number of available charging stations for SAEVs at any given time period is $C_h - c_{ht}$, hence we have that:

$$\sum_{b\in\mathcal{B}} (w^{b+}_{ht} + w^{b-}_{ht}) \leq C_h - c_{ht} \qquad \forall h \in \mathcal{H}, t \in \overline{\mathcal{T}}. \tag{23}$$

We consider that the SAEVs can park at city parking lots, which has cost α_p for each time period it stays parked. The CPS operator pays the unit cost of electricity consumed (π_{ht}) to the SO. The revenue for the fleet and the hub system comes from three sources, namely, energy sold to the grid (at the rate π_{ht}), payments from privately owned EVs, and payments received from the passengers (ψ_t per time period on the road). Then, the hubs operational model can be formulated as:

$$\begin{aligned}
\max \; & \sum_{t\in\overline{\mathcal{T}}} \sum_{b\in\mathcal{B}} \sum_{(i,j)\in\mathcal{A}} \psi_t \tau_{ij} x^b_{ijt} - \sum_{p\in\mathcal{P}} \sum_{t\in\overline{\mathcal{T}}} \sum_{b\in\mathcal{B}} \alpha_p z^b_{pt} \\
& - \sum_{h\in\mathcal{H}} \sum_{t\in\overline{\mathcal{T}}} \pi_{ht} \left(\sum_{b\in\mathcal{B}} \left(g^b_{ht} - p^{b-}_{ht}\right) + g_{ht} - \hat{p}^-_{ht} - f^-_{ht} + g^{\text{EV}}_{ht} \right) \\
& + \sum_{h\in\mathcal{H}} \sum_{t\in\overline{\mathcal{T}}} \pi_{ht} P^+ c_{ht} + \sum_{h\in\mathcal{H}} \sum_{t\in\overline{\mathcal{T}}} \zeta_h c_{ht}
\end{aligned} \tag{24}$$

s.t., (1)–(23)

The objective function (24) has five components that accounts for the following:

1. fare received from the passengers,
2. parking fee paid by the idling SAEVs,
3. total payment by the CPS to the system operator for consumption of electricity; negative elements denote the payment received by the CPS,
4. payment received by the CPS from the privately owned EVs for energy consumed, and
5. payment received by the CPS from the privately owned EVs for occupying the charging stations.

We solve two modified versions at different stages of the methodology. First, we solve a deterministic version of the model in the "Ad hoc load schedule" step, and then we robustify the model in the second stage of the methodology. In what follows, we describe each of the steps of the methodology.

4.3 Ad hoc load Schedule and Market Clearing Price Estimation

The ad hoc load schedules developed using the planning model serve as input for the day-ahead commitment model, which is described later. A few parameters of our model that are required for this step are: price of electricity paid by the CPS (π_{ht}), charging demand of the privately owned EVs (W^v_{ht}), available solar power (F_{ht}), and the number of passenger arrivals (γ_{ijt}). All the above parameters are stochastic. We construct distributions for these parameters based on prior information, and generate random samples of the vector $\mathcal{V} = \{\pi_{ht}, W^v_{ht}, F_{ht}, \gamma_{ijt}\}$, $\forall i \in \overline{\mathcal{N}}, j \in \overline{\mathcal{N}}, t \in \overline{\mathcal{T}}, h \in \mathcal{H}$. Then, we obtain the minimal-cost load schedule for each hub and for any given realization of $\mathcal{V}$ as $D_{ht} = \sum_{b \in \mathcal{B}} g^{b*}_{ht} + g^{*}_{ht} + g^{EV*}_{ht}$ for all $h \in \mathcal{H}, t \in \overline{\mathcal{T}}$, where the optimal values of the variables are obtained from the solution of (24), subject to (1)–(23). Let $\mathcal{V}^l$ be a realization of the random vector $\mathcal{V}$. Then, we denote the set of minimal cost load schedule scenarios for each hub h as $\mathcal{D}_h = \{D_{ht}(\mathcal{V}^l) : t \in \overline{\mathcal{T}}, l \in \{1, \cdots, N\}\}$, where N is the number of randomly selected samples of $\mathcal{V}$. We select a relatively large value for N so that the variations of the components of $\mathcal{V}$ are well represented in the samples.

To reduce the computational burden of the subsequent DA commitment process, we select a representative subset of the ad hoc load schedules, using a scenario reduction technique adopted form Growe-Kuska et al. (2003). This technique selects a subset of the load scenarios, denoted by Ω, and assigns to each a probability of occurrence μ^ω, $\forall \omega \in \Omega$. We use the load schedule D^ω_{ht} and the generators DA bids to solve the ACOPF model presented in Appendix A. Solution of the ACOPF model yields an estimate of the day-ahead market clearing prices (MCP^ω_{nt}) at each bus $n \in \mathcal{N}$, where $\mathcal{N}$ is the set of all buses in the power network. The ACOPF model is solved in practice for each hour of the day, though our operational model has shorter time periods. Hence, to solve the ACOPF model for each hour, we sum the loads of all time periods within the hour. Note that, more than one hub may be directly connected to a single bus in the grid. The total real and reactive power load at each bus is equal to the sum of all the loads connected to the bus (houses, industries, the hubs, etc.). The real power load of each hub h, in a given scenario w, is equal to D^ω_{ht}, while the reactive power demand is a fraction of D^ω_{ht}.

4.4 Two-Stage Stochastic Model for Day Ahead Commitment

In this subsection, we present our two-stage stochastic model for obtaining DA commitment for each hub as discussed in step 3 of the methodology presented in Section 3. The model requires both DA and RT prices,

where the DA prices are the MCPs obtained in step 2. These DA prices in turn are used to estimate the RT prices; for this, we use the method proposed in Das & Wollenberg (2005), which is summarized below. The RT prices at bus n are estimated as $\pi^{\omega}_{nt} = \text{MCP}^{\omega}_{nt}[1+\epsilon]$, where $\epsilon = M_1\epsilon_1 + M_2\epsilon_2$; ϵ_1 and ϵ_2 are random variables and are drawn from normal and Cauchy distributions, respectively, and (M_1,M_2) is a bivariate random variable that takes value of $(0,1)$ with probability p_s and (1,0) with probability $(1-p_s)$, where p_s denotes the probability of occurrence of price spikes. The normal random variable ϵ_1 captures the usual variability in the real time prices, whereas the Cauchy random variable ϵ_2 generates the price spikes. The load schedules of each hub (D^{w}_{ht}), the estimated market clearing prices (MCP^{w}_{nt}), and the corresponding real time prices (π^{ω}_{nt}), are used to formulate the two-stage stochastic model as follows.

The two-stage model assumes that each hub can either sell or buy excess or shortfall quantities in the RT market. Let p^{DA}_{ht} denote the quantity committed in the DA market by hub h at time period t. Then, the hourly DA commitment is equal to the sum of the p^{DA}_{ht} for all time periods belonging to the hour. Let $p^{\omega,RT+}_{ht}$ and $p^{\omega,RT-}_{ht}$ be the quantities bought and sold, respectively, in the RT market, by hub h at time period t in scenario $\omega \in \Omega$. Then, the DA commitment for the hubs are obtained by solving the following cost minimization model.

$$\begin{aligned} \min \quad & \sum_{\omega\in\Omega} \mu^{\omega} \Big[\sum_{t\in\mathcal{T}} \sum_{n\in\mathcal{N}} \sum_{h\in\mathcal{H}_n} \Big(\text{MCP}^{\omega}_{nt} p^{\text{DA}}_{ht} + \pi^{\omega}_{nt} p^{\omega,RT+}_{ht} - (\pi^{\omega}_{nt} - \delta^{\text{RT}}) p^{\omega,RT-}_{ht} \Big) \Big] \\ \text{s.t.,} \quad & p^{\text{DA}}_{ht} + p^{\omega,RT+}_{ht} - p^{\omega,RT-}_{ht} = D^{\omega}_{ht}, \qquad \forall h \in \mathcal{H}, t \in \overline{\mathcal{T}}, \omega \in \Omega, \end{aligned} \tag{25}$$

where $\mathcal{H}_n$ is the set of hubs directly connected to bus n, and δ^{RT} is a penalty for not using the DA committed quantity. The first two terms of the objective function denote the cost of purchasing electricity from the DA and RT markets. The third term takes into account selling of excess electricity in the RT market. The constraint accounts for the conservation of power by equating effective quantity of electricity purchased to the demand.

4.5 Real Time operational model

This final element of our methodology (stage 2) comprises a real-time operational model that guides the actions of the SAEVs and the hubs. The real-time operational model is a robust version of the planning model presented in Section 4.2. Note that, unlike stage 1 of our methodology which uses ad hoc load schedules and estimated prices based on historical data, the real time model uses observed parameters in real time for each time period of the day. In what follows, we present some additional constraints that are needed to incorporated the DA commitment. Once the DA commitment for the hubs is made, the SO discloses the DA prices, π^{DA}_{ht}, and the CPS operator pays $\sum_{h\in\mathcal{H}} \sum_{t\in\overline{\mathcal{T}}} \pi^{\text{DA}}_{ht} p^{\text{DA}}_{ht}$. Since, based on the DA commitment, any shortfall or excess is procured in the RT market, we can write that

$$g^{b}_{ht} = g^{b,\text{DA}}_{ht} + g^{b,\text{RT}}_{ht}, \qquad \forall h \in \mathcal{H}, t \in \overline{\mathcal{T}}, b \in \mathcal{B}, \tag{26}$$

$$g_{ht} = g^{\text{DA}}_{ht} + g^{\text{RT}}_{ht}, \qquad \forall h \in \mathcal{H}, t \in \overline{\mathcal{T}}, \tag{27}$$

$$g^{\text{EV}}_{ht} = g^{\text{EV,DA}}_{ht} + g^{\text{EV,RT}}_{ht}, \qquad \forall h \in \mathcal{H}, t \in \overline{\mathcal{T}}. \tag{28}$$

The DA commitment is used to 1) charge the batteries of the SAEVs, privately owned EVs, and the battery bank and 2) sell it in the RT market if profitable, i.e., if the RT prices are high, the hubs may use

their DA commitment to arbitrage in the RT market. Then, we can write the following.

$$\sum_{b\in\mathcal{B}} g_{ht}^{b,\mathrm{DA}} + g_{ht}^{\mathrm{DA}} + g_{ht}^{\mathrm{EV,DA}} + p_{ht}^{\mathrm{RT}-} = p_{ht}^{\mathrm{DA}}, \qquad \forall h \in \mathcal{H}, t \in \overline{\mathcal{T}}, \tag{29}$$

where $p_{ht}^{\mathrm{RT}-}$ is the actual quantities sold to the RT market by hub $h \in \mathcal{H}$ at time period $t \in \overline{\mathcal{T}}$. Selling back to the grid not only benefit the system of hubs (economically), but also help the system operator to match demand and supply; RT prices are rise when the current demand in the network is higher in comparison to the supply.

To simplify the formulation of the real-time operational model, we define the dummy variables a^{RT} and a_b^{RT} as:

$$a^{\mathrm{RT}} = \sum_{h\in\mathcal{H}} \sum_{t\in\overline{\mathcal{T}}} \pi_{ht}^{\mathrm{RT}} l_{ht}^{\mathrm{RT}}, \tag{30}$$

$$a_b^{\mathrm{RT}} = \sum_{h\in\mathcal{H}} \sum_{t\in\overline{\mathcal{T}}} \pi_{ht}^{\mathrm{RT}} l_{ht}^{b,\mathrm{RT}}, \qquad \forall b \in \mathcal{B}, \tag{31}$$

where l_{ht}^{RT} and $l_{ht}^{b,\mathrm{RT}}$ are dummy variables defined as:

$$l_{ht}^{\mathrm{RT}} = P^{+} c_{ht} + \hat{p}_{ht}^{-} + f_{ht}^{-} - g_{ht}^{\mathrm{RT}} - g_{ht}^{\mathrm{EV,RT}}, \qquad \forall h \in \mathcal{H}, t \in \overline{\mathcal{T}}, \tag{32}$$

$$l_{ht}^{b,\mathrm{RT}} = p_{ht}^{b-} - g_{ht}^{b,\mathrm{RT}}, \qquad \forall b \in \mathcal{B}, h \in \mathcal{H}, t \in \overline{\mathcal{T}}. \tag{33}$$

Finally, to account for the fraction of the DA commitment that is sell back to the grid we define

$$a^{\mathrm{DA}} = \sum_{h\in\mathcal{H}} \sum_{t\in\overline{\mathcal{T}}} (\pi_{ht}^{\mathrm{RT}} - \delta^{\mathrm{RT}}) p_{ht}^{\mathrm{RT}-}. \tag{34}$$

Then, we can re-write the objective function (24) at any time period $\tau \in \overline{\mathcal{T}}$ as:

$$\max \qquad \sum_{t=\tau}^{|\overline{\mathcal{T}}|} \sum_{b\in\mathcal{B}} \sum_{(i,j)\in\mathcal{A}} \psi_t \tau_{ij} x_{ijt}^{b} + a^{\mathrm{RT}} + \sum_{b\in\mathcal{B}} a_b^{\mathrm{RT}} + a^{\mathrm{DA}} + \sum_{h\in\mathcal{H}} \sum_{t\in\overline{\mathcal{T}}} \zeta_h c_{ht} - \sum_{t=\tau}^{|\overline{\mathcal{T}}|} \sum_{p\in\mathcal{P}} \sum_{b\in\mathcal{B}} \alpha_p z_{pt}^{b}. \tag{35}$$

The abode objective function is subjected to constraints (2)–(18), (21)–(23), (26)–(29), (32) and (33), in which we must now replace $\forall t \in \overline{\mathcal{T}}$ by $\forall t \in \{\tau, \cdots, |\overline{\mathcal{T}}|\}$. Additionally, the model is also subjected to the robust versions of those constraints with uncertain parameters, namely, constraints (1), (19), (20), (30), and (34). In Appendix B, we show the robust counterparts of these constraints. Note that, the cost of electricity procured through DA commitment ($\sum_{h\in\mathcal{H}} \sum_{t\in\overline{\mathcal{T}}} \pi_{ht}^{\mathrm{DA}} p_{ht}^{\mathrm{DA}}$) is subtracted from the optimal objective value of (35) to obtain the final gross profit of the CPS.

5 A Case Study

We demonstrate our methodology by implementing it on a sample problem where a CPS operates within a city's transportation and power networks. A schematic representation of the CPS is given in Figure 3. The network on the right represents the transportation network with 12 nodes, 5 hubs, and the connecting arcs. The case study uses actual transportation demand data for the City of Tampa, and the demands are aggregated for zones at which nodes are located. The Tampa Bay area is represented by 12 such transportation

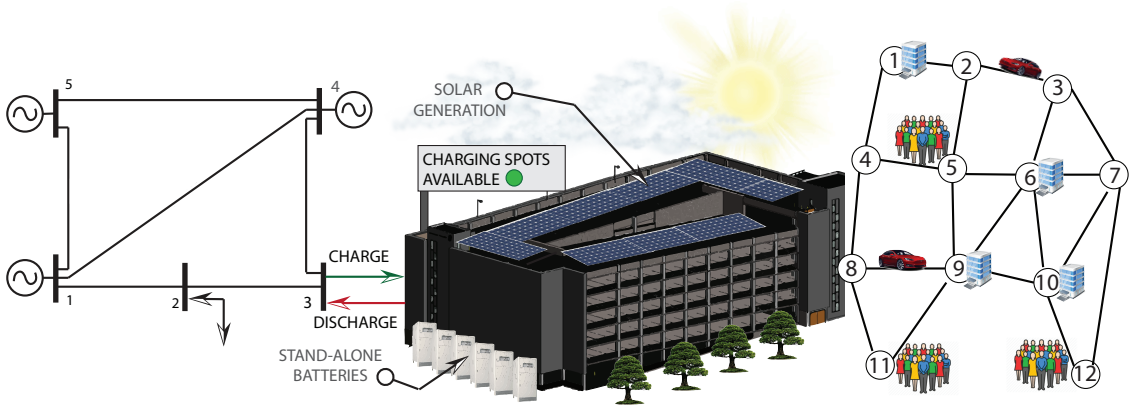

Figure 3: Schematic of a CPS interacting with power and transportation networks

nodes. The building in the middle represents one of the charging/discharging hub with its PV generation and bank of stand alone batteries. The hub is connected to one a bus of the power network which is abstracted as a 5 bus network as shown on the left. We used a simplified power network similar to that of PJM's 5-bus network to represent the power supply scenario.

The CPS is considered to have the following features. It has a fleet of 500 SAEVs, each with a battery size of 100 kWh and a range efficiency of 0.293 kWh per mile on city roads (similar to Tesla model S). The SAEV fleet is supported by a system of five hubs, each with 50 super-chargers with an hourly charge/discharge rate of 70kW for each charger. Each hub has a stand-alone battery bank with a capacity of 600 kWh and an hourly charge/discharge rate of 300 kW. Each hub is also considered to have a solar generation facility with a peak capacity of 200 kW. The PV generation capacities at the charging hubs are assumed based on estimated roof area of the charging hubs and actual solar irradiance values for the Tampa Bay region. Generation from these PV units across the day is modeled using the patterns obtained from Tampa Electric Company (TECO) serving the city of Tampa, Florida, U.S. The CPS serves passenger transportation in the city of Tampa and its suburbs. For ease of computation, the origins and destinations (ODs) of the transportation network are clustered into twelve nodes as shown in Figure 4a. A similar clustering approach was used in Iacobucci et al. (2019). The hubs are considered to be located in five of the twelve node locations (1, 6, 8, 9 and 10). The locations for the five hubs were chosen somewhat arbitrarily from among 12 transportation nodes based on demand volume and distance from other nodes with no hubs. The average travel time from each hub to the rest of the service area are depicted in heat maps in Figure 4b to Figure 4f; the travel time data is adopted from Uber (2020). Based on the travel time data, we assumed that all travel times are multiples of 15 minutes apart and the maximum trip duration is 75 minutes; every 15 minutes is considered one time period in our model. The transportation demands served by the SAEVs for each time period are generated using the actual daily travel requests in Tampa; we assume that 30% of all passenger travel requests are potential customers for the SAEVs. The distribution of the total daily demand over the time periods of a day is considered to be same as in Zhou et al. (2003). For charging demand of privately owned EVs, we use the arrival patterns and fleet composition as presented in Subramanian & Das (2019). EVs request charging for up to four time periods, and once accepted to a hub they remain charging till the request is fulfilled. The privately owned EVs pay to the hub a facility fee ($8/hour) plus the prevailing real time price of electricity. The SAEVs receive $45/hour for transporting passengers and when idle and park they pay a parking fee of $10/hour.

The power grid to which the CPS is connected is considered to be the modified PJM 5-bus network, as

Table 1: Generator cost functions used in the case study

Generator	Cost function	Generator	Cost function
1a	$0.100P_g^2 + 12P_g + 100$	4c	$0.100P_g^2 + 19P_g + 70$
1b	$0.100P_g^2 + 20P_g + 30$	5a	$0.100P_g^2 + 17P_g + 60$
1c	$0.100P_g^2 + 08P_g + 40$	5b	$0.120P_g^2 + 18P_g + 50$
4a	$0.100P_g^2 + 10P_g + 50$	5c	$0.085P_g^2 + 20P_g + 80$
4b	$0.100P_g^2 + 25P_g + 150$		

shown in Figure 3. The network has the two load buses (2 and 3) and three generating buses (1, 4, and 5) each with three identical generators of 800 MW capacity. The characteristics of the six transmission lines (capacity, reactance, and susceptance) are adopted from Li & Bo (2010). The generator cost functions are assumed to be quadratic with parameters presented in Table 1, which are obtained from Das & Wollenberg (2005). The base load of the 5-bus network (not considering the load of the CPS) is considered to be same as the DAY zone of the PJM network (U.S.) for the time period between July 15, 2019 and July 30, 2019; we consider summer days only to avoid seasonal variability.

For implementing our methodology, we need historical data for transportation demand, electricity price, PV generation at the hubs, and EV charging demand. For these parameters, we developed probability distribution for each time period of a day using the available data from the sources described above. We use normal distribution for the nodal electricity prices and PV generation, and Poisson distribution for the transportation and EV charging demands. We then draw one hundred samples for all time periods from each of these distributions and solve (24), as described in Section 4.3, to generate the ad hoc load scenarios. The scenario reduction technique is then used to obtain ten representative ad hoc load scenarios with respective probabilities. For each of these ten load scenarios along with the base load of the city, we solve the ACOPF model (43) to estimate the DA MCPs and then derive the RT prices at each load bus. Hereafter, considering the selected load and price scenarios with their corresponding probabilities, we solve the two-stage model (25) to obtain the hourly DA commitment for each hub. Using these DA commitments, we solve the real time operational model in (35). We implement our methodology on the sample problem using Julia 0.7.1 as programming language and GUROBI 9.0.0 as optimization solver. The results are organized to address three key goals of our numerical study: 1) to demonstrate that our methodology is capable of yielding real-time operational strategies for the CPS, 2) to demonstrate the influence of power network on CPS operation, and 3) to measure the added financial benefit to CPS that is made possible by the detailed power network considerations in our methodology (unlike the existing literature).

Our methodology was successful in obtaining real time action choices for the CPS elements (SAEVs, hubs, battery banks, and PV generators) for all 96 time periods of a day. Some of these action choices are depicted in the figures that are discussed next. Figure 5a illustrates the distribution of the SAEVs arriving at the nodes throughout the day (vehicles in between nodes are not included). Although, in our implementation, all the SAEVs were assigned to be at hub nodes (100 in each) at time period 1, it can be seen that the vehicles are well distributed across the city during the day. The maximum aggregated number of SAEVs arriving at the nodes at any time period is observed to be less than 40% of the fleet size, meaning 60% or more of the SAEVs are traveling between nodes. The SAEVs served a total of 10,288 trips during the day out of 53,441 trips generated. This indicates that the fleet size of 500 is inadequate for the demand considered here. Figure 5b shows the number of SAEVs charging at the hubs (at nodes 1, 6, 8, 9, and 10) throughout the day. Average occupancy of the hubs is observed to be around 35 vehicles. Hence, a system of five hubs with

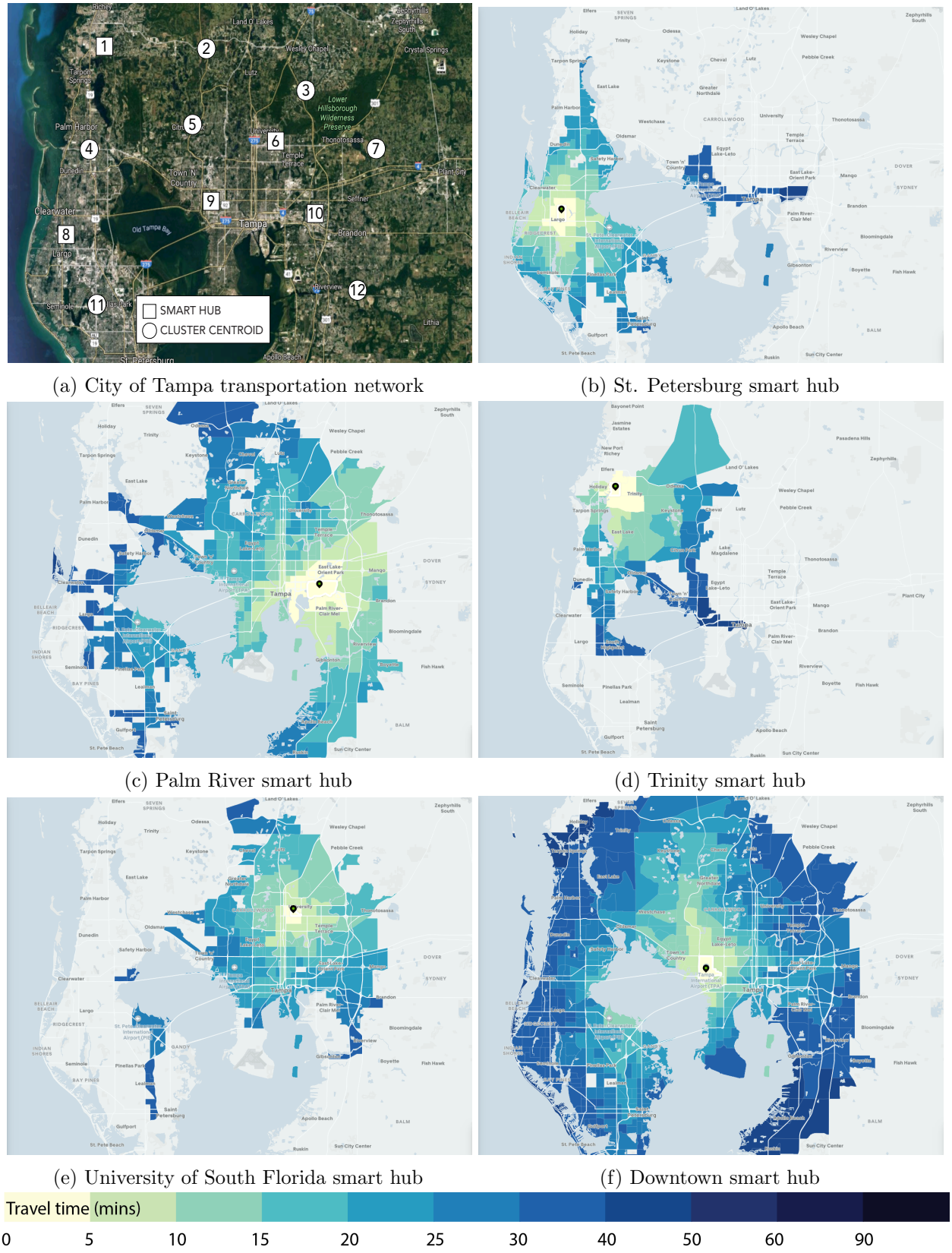

(a) City of Tampa transportation network

(b) St. Petersburg smart hub

(c) Palm River smart hub

(d) Trinity smart hub

(e) University of South Florida smart hub

(f) Downtown smart hub

Figure 4: Simplified City of Tampa transportation network and location of the smart hubs

50 charging stations in each is generally underutilized for a fleet size of 500; only the hub at node 8 can be observed to be fully occupied for a few time periods of the day. This indicates that there is available capacity for the CPS to offer charging services to privately owned EVs. Figure 5c shows the number of privately owned EVs that were allowed to charge at the hubs, as determined by the optimal solution. Note that the pattern of EV charging demand, adopted from Subramanian & Das (2019), is mostly concentrated during the morning hours, which explains the result in Figure 5c. Figure 5d shows the number of SAEVs idling (neither serving trips, traveling empty, nor charging). SAEVs can be seen to idle only at the hub nodes and at those time periods when higher numbers of EVs are allowed at the hubs. The total idle time of the SAEVs is less than 1.6%, which aligns well with the fact that the demand for trips in the system is very high for the given fleet size. We noted that our methodology generated a total gross profit of $229,193 per day, which includes $3,494 from serving the privately owned EVs and $2498 from arbitrage using the battery banks. Hence, optimal operation of the CPS with 500 SAEVs and five hubs of 50 charging station could generate an estimated annual gross profit close to 84 million dollars. However, this estimate is high for the following reasons: 1) the trip demand for the sample problem is too high for a fleet size of 500 and hence there is little to no idle time for the vehicles, 2) no time lag is accounted for between drop off and pick up when a passenger is available at a node, 3) no time loss for connecting/disconnecting vehicles at the hubs is considered, and 4) outages for vehicle break down and maintenance are not included.

Since our methodology does not address how to select the optimal capacities for the hubs that are needed for the system, we conducted a sensitivity analysis. For a number of different fleet sizes, between 100 and 500, we determined the approximate number of charging stations in each of the five identical hubs, beyond which the gross profit of the CPS did not seem to increase significantly. We approximated this point using the fit3 technique presented in Smith & Corripio (1997). We plotted the optimal number of charging stations (in all five hubs combined) per SAEV for different values of the fleet size, see Figure 6. It shows that the average number of charging stations needed per vehicle is 0.41 (with a standard deviation of 0.038).

Recall that, the second goal of our case study was to measure the influence of power network on the CPS operation. For this, we plotted the total grid consumption by the hubs, the total DA commitment for the hubs, and the RT prices. Note that, the DA commitment and the RT prices largely guide the charging strategy. The plots are shown in Figure 7 for only two hubs (1 and 10) that are connected to two different load buses in the sample power network. In these figures, the bars indicate the total DA commitment by the hubs for each time period, the red line represents the RT prices, and the bold line shows the energy consumed by the hubs from the grid. Figure 7a depicts the results for the case in which privately owned EVs are not allowed to charge at the hubs. We notice that the energy consumption from the grid is closely aligned with the DA commitment, which means that the CPS operator is able to hedge effectively against the RT price risk through its two-stage stochastic DA commitment model. The consumption from the grid can be seen to be generally slightly higher that the DA commitment. However, at some of the time periods, say 24-36 (in hub 1) and 65-70 (in hub 10) when the RT prices are higher, the DA commitment chosen by the model is larger than actual consumption. By doing so, the model has created opportunities for arbitrage, where the excess commitment is sold back to the RT market for profit. We notice however that the energy arbitrage potential of the sample CPS, with only 500 vehicles serving a transportation network with a significantly high passenger demand, is very limited as the revenue from passenger fare is much higher than that from energy arbitrage. Figure 7b presents results for the scenario when privately owned EVs are allowed to charge at the hubs. We have seen earlier in Figure 5c that more EVs charge at the hubs in the early morning hours of the day (around time period 30 to 40; 7:30 AM to 10:00 AM), hence for both hubs 1 and 10, the DA commitment as well as the grid consumption are much higher in the early hours (see Figure 7b); the remainder of the day

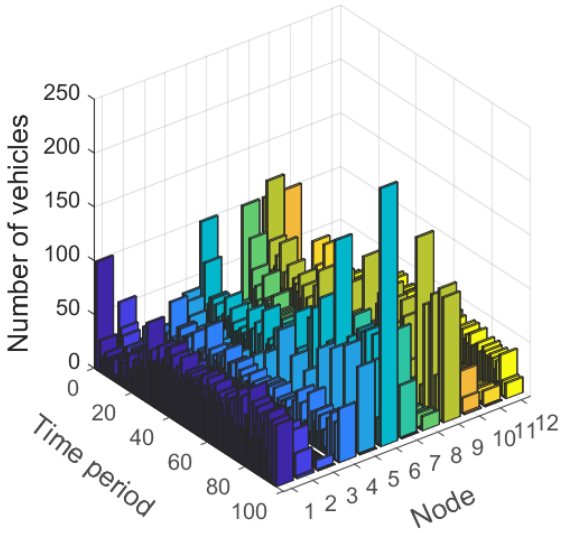

(a) Arrival of SAEVs

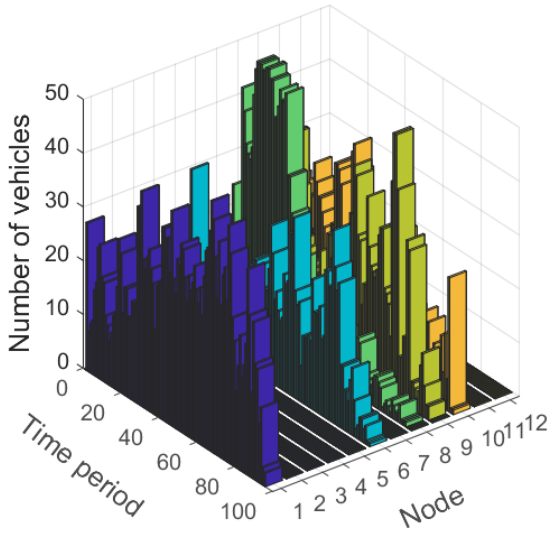

(b) Number of SAEVs charging

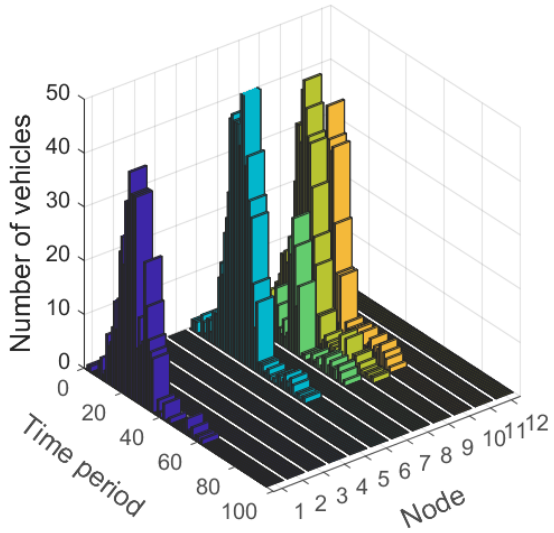

(c) Number of EVs charging

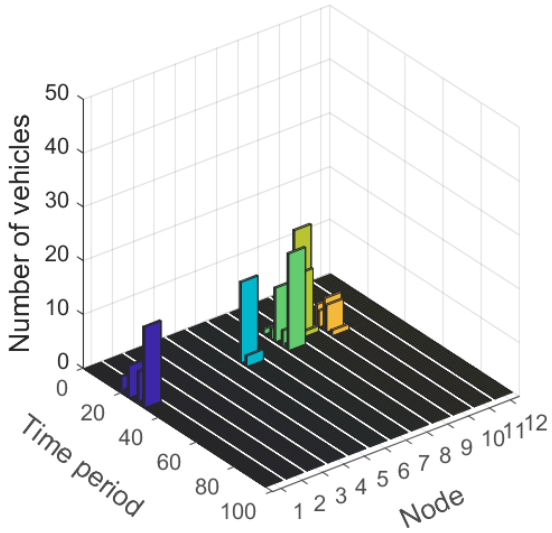

(d) Idle SAEVs

Figure 5: Distribution of SAEVs and charging patterns of SAEVs and EVs

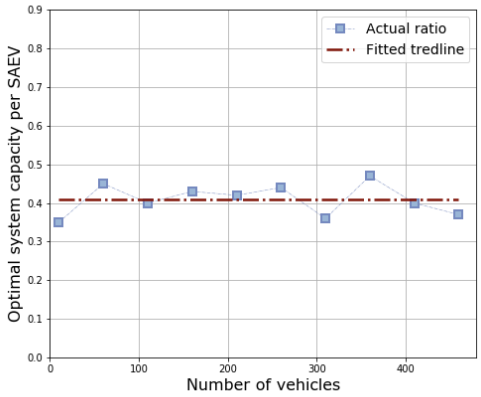

Figure 6: Optimal ratio of hub capacity to number of vehicles in the fleet

they are similar to Figure 7a.

We address the third goal of our numerical study by assessing the additional financial benefits generated by considering power network aspects. This was accomplish by measuring the cost savings attained by the hubs by buying power through optimal DA commitments for different levels of RT price variations. Recall that the DA commitment requires solution of the ACOPF model via steps 1-3 of our methodology. We obtained the operational strategies for the CPS using two approaches: 1) by using the complete methodology including optimal DA commitment, and 2) by eliminating DA commitment and paying RT prices for all consumption from the grid by the hubs. The increase in gross profit of the CPS by using optimal DA commitment (as opposed to paying RT prices for the whole quantity) was assessed for a number of scenarios with an increasing level of RT price spikes; these spikes were generated by increasing the location parameter of the Cauchy distribution. Note that, the location parameter is the median/mode value of the price spike, and as in Das & Wollenberg (2005), the scale parameter was kept same as the location parameter. We plotted the increase in gross profit with increasing RT price spikes (see Figure 8). As expected, in the absence of price spikes, i.e., when the location and scale parameter values are zero, the increase in gross profit from using DA commitment is negligible. However, as the intensity of price spikes increases (with increasing location parameter value), DA commitment yields an increasing level of gross profit. For a typical range of RT price spikes in the U.S. electricity markets, for which the location parameter tends to lies between \$0.2/kWh to \$0.4/kWh, the CPS can achieve an increase in the gross profit between \$2000 to \$3000 per day.

5.1 Comments on computational challenges

Recall that, the part of our methodology that addresses the transportation aspect uses a variant of an existing model (Zhang et al. 2016). However, we have reformulated the constraints in Zhang et al. (2016) and our version of the transportation model uses a significantly less number of binary variables. Though this reduction makes our methodology easier to solve, the computational times for both the planning and the real time operational models still increase exponentially with the fleet size. This is due to the fact that even when the number of integer variables in our methodology grows linearly with the fleet size, computation time for mixed integer programs (MIPs) increases exponentially with the number of integer variables. Furthermore, in our methodology we need to solve many iterations of the planning model, which is needed to capture

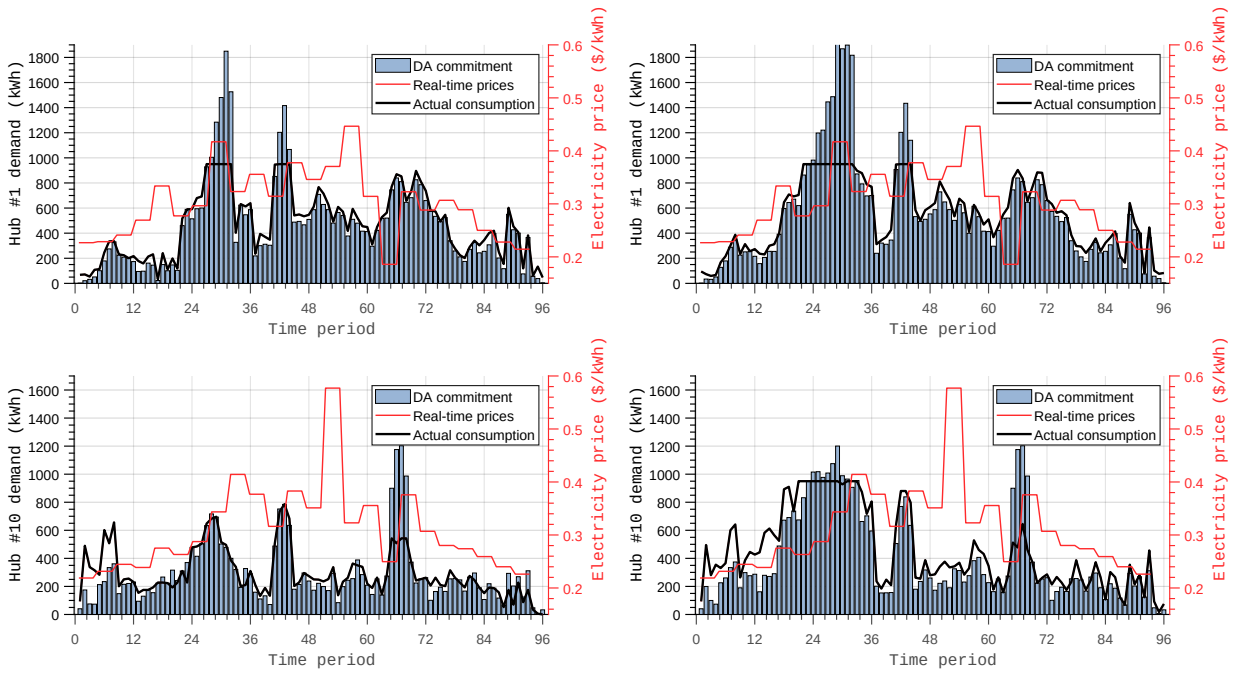

(a) Without privately owned EVs

(b) With privately owned EVs

Figure 7: Comparison of DA commitment with actual consumption for selected hubs

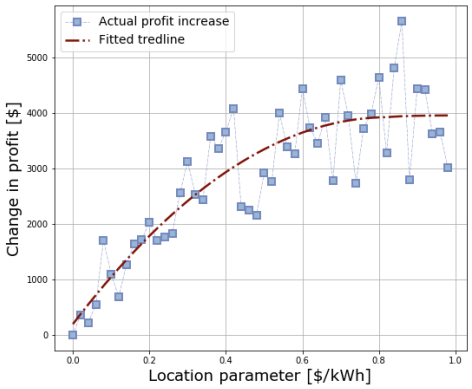

Figure 8: Financial benefits of DA commitment with increasing RT price spikes

the variability of the electricity price, transportation demand, solar generation, and charging demand of the privately owned EVs. Hence, solving the planning model is computationally burdensome, especially for large fleet sizes. We have also observed that with smaller hub capacities, finding acceptable solutions of the MIP models in our methodology becomes difficult using commercial optimization solvers (like GUROBI). We conjecture that this occurs because the number of feasible schedules for the SAEVs decreases with reduced hub capacities; this is analogous to the findings reported in studies that compared uncapacitated and capacitated facility location problems, e.g., Verter (2011). As we have discussed earlier, the fleet size of 500 is very small for the level of transportation demand in the CPS of our case study, and also five hubs of capacity fifty is perhaps more than what is optimal for a fleet of 500 SAEVs. Hence, we have develop a simpler modified (myopic) approach for the planning and operational models of our methodology. It is expected that this myopic approach can to obtain near-optimal solutions more efficiently for systems with larger fleet sizes and limited hub capacities.

6 A myopic approach for planning and operational decisions

The myopic alteration of our methodology applies to both the model for obtaining ad hoc load schedules (in step 1) and real time operational strategies (in step 4). For step 1, the myopic approach works as follows. Instead of finding the operational strategies of SAEVs, battery banks, and EVs using a single optimization model, we obtain those sequentially, as follows. First, we optimize the charge/discharge schedule of the battery banks at all hubs by considering the electricity prices only, i.e., guided by temporal arbitrage alone. Then, we use this charge/discharge schedule of the battery banks, expected PV generation, and historical electricity prices to determine the actions of the SAEVs that are not committed at each time period of the day. Thereafter, we decide the number of privately-owned EVs that are allowed to enter the hubs at each time period of the day. The above sequential approach determines the ad hoc load schedule (i.e., how much power to buy from the grid). Note that, the energy discharged from the battery banks and the generation by the PV are prioritized for use first by the SAEVs and then EVs; any unused quantity is injected back to the grid. For step 4 of our methodology, the myopic approach works in a similar manner as for step 1. The main difference being that instead of using historical electricity prices, we use DA commitment and RT prices (along with discharge schedule of battery banks and PV generation) to obtain actions for SAEVs not committed to other tasks in each time period.

6.1 A Myopic model for selecting actions for SAEVs

We solve a sequence of (modified) linear assignment problems to decide the next action of SAEV b. Let $\hat{x}^b_{ij}$, $\hat{z}^b_i$, $\hat{w}^{b+}_h$, and $\hat{w}^{b-}_h$ be equal to 1 if SAEV b is assigned to 1) pick a customers from i to j, 2) park at node i, 3) charge at hub h, and 4) discharge and hub h, respectively, and 0 otherwise. Then, at each time period we

can solve the following optimization model.

$$
\begin{aligned}
\max \quad & \sum_{(i,j)\in\mathcal{A}}\sum_{b\in\mathcal{B}} \psi_{ij}^{b}\hat{x}_{ij}^{b} - \sum_{i\in\overline{\mathcal{N}}}\sum_{b\in\mathcal{B}} \alpha_{i}^{b}\hat{z}_{i}^{b} - \sum_{h\in\mathcal{H}}\sum_{b\in\mathcal{B}} \pi_{h}^{b+}\hat{w}_{h}^{b+} + \sum_{h\in\mathcal{H}}\sum_{b\in\mathcal{B}} \pi_{h}^{b-}\hat{w}_{h}^{b-} \\
\text{s.t.,} \quad & \sum_{(i,j)\in\mathcal{A}} \hat{x}_{ij}^{b} + \sum_{i\in\overline{\mathcal{N}}} \hat{z}_{i}^{b} + \sum_{h\in\mathcal{H}} \left(\hat{w}_{h}^{b+} + \hat{w}_{h}^{b-}\right) = 1 \quad \forall b \in \mathcal{B} \\
& \sum_{b\in\mathcal{B}} \hat{x}_{ij}^{b} \leq d_{ij} \quad \forall (i,j) \in \mathcal{A} \\
& \sum_{b\in\mathcal{B}} \left(\hat{w}_{h}^{b+} + \hat{w}_{h}^{b-}\right) \leq \hat{C}_{h} \quad \forall h \in \mathcal{H} \\
& 0 \leq \hat{x}_{ij}^{b}, \hat{z}_{i}^{b}, \hat{w}_{h}^{b+}, \hat{w}_{h}^{b-} \leq 1
\end{aligned}
\tag{36}
$$

where, ψ_{ij}^{b}, α_{i}^{b}, π_{h}^{b+}, and π_{h}^{b-} denote the unit values for the revenue of vehicle b from transporting a customer from i to j, cost of parking at node i, cost of charging at hub h, and revenue from discharging and hub h, respectively. These values depend on the time when each SAEV completes its assigned action; we denote this completion time as θ. To compute the above parameters, we define the minimum state of charge that an SAEV must maintain at a completion of a task. For example, the minimum state of charge of any vehicle completing a task at node k is given by $s_{k}^{\min} = \underline{S}_{b} + \frac{1}{\phi_{b}}\tau_{kh}\epsilon_{b}$, where hub h is the closest to node k. Then, the revenue from transporting a customer in i to j can be given as:

$$
\psi_{ij}^{b} = \begin{cases} \psi_{ij}\tau_{ij}, & \text{if } s_{\theta}^{b} \geq s_{j}^{\min} \\ -M, & \text{otherwise,} \end{cases}
\tag{37}
$$

where M is a big positive number. The cost for parking at node i is given as,

$$
\alpha_{i}^{b} = \begin{cases} \alpha_{i} + L, & \text{if } s_{\theta}^{b} \geq s_{i}^{\min} \\ M, & \text{otherwise,} \end{cases}
\tag{38}
$$

where L is a positive number chosen to make the perceived cost of parking higher than the average cost of electricity. This is done to allow SAEVs, without a customers to serve, to choose charging instead of parking unless the price of electricity is expected to be even higher in the current time period. The cost of discharging can be written as,

$$
\pi_{h}^{b-} = \begin{cases} \pi_{h\theta}\, \min\{P^{-}, \phi^{b}(s_{\theta}^{b} - \underline{S}^{b})\}, & \text{if } s_{\theta}^{b} \geq s_{h}^{\min} \\ -M, & \text{otherwise.} \end{cases}
\tag{39}
$$

In a similar manner, the cost of charging can be written as,

$$
\pi_{h}^{b+} = \begin{cases} \bar{\pi}_{h\theta}\, \min\{P^{+}, \phi^{b}(\overline{S}^{b} - s_{\theta}^{b})\}, & \text{if } s_{\theta}^{b} \geq s_{h}^{\min} \\ M, & \text{otherwise.} \end{cases}
\tag{40}
$$

Note that the cost of discharging is calculated using the electricity price at the time of arrival to the hub, $\pi_{h\theta}$, whereas for the cost of charging we use $\bar{\pi}_{h\theta}$, which is given as,

$$
\bar{\pi}_{h\theta} = \max\left\{\frac{C_{h} - N_{h\theta}}{C_{h}}, 0\right\}\pi_{h\theta}, \qquad \forall h \in \mathcal{H},
\tag{41}
$$

where,

$$N_{h\theta} = \left\lfloor \frac{F_{h\theta} + P^{-}_{h\theta} + P^{\mathrm{DA}}_{h\theta}}{P^{+}} \right\rfloor \tag{42}$$

is the maximum number of vehicles that can be charged using the combination of the available solar power, the discharged power from the bank of strand-alone batteries, and the DA commitment. The logic behind (41) is as follows. For simplicity, assume that $N_{h\theta} \leq C_h$ and that all charging stations (C_h) are assigned to be used at time θ. Then, the assigned SAEVs will pay $0 \times N_{h\theta} + \pi_{h\theta} \times (C_h - N_{h\theta})$. Hence, we have that $\frac{C_h - N_{h\theta}}{C_h}\pi_{h\theta}$ is the average price paid by the SAEVs if all charging stations are used. Considering that $N_{h\theta}$ might be greater that C_h leads to Equation (41). Hence, we are assigning SAEVs to charge assuming they will pay the average price.

7 Results from the case study using the myopic approach

We first assess the performance of the myopic approach by comparing its computation time and gross profit with those obtained from the original version of our methodology. All computational experiments are carried out on a Dell Optiplex 9020 with Intel(R) Core(TM) i7-4790 CPU @ 3.60 GHz, 4-core processor, 16 GB RAM, and Microsoft Windows 10 Enterprise operating system. We first assessed the savings in computation time for a number of fleet sizes ranging from 50 to 500. Recall that the myopic approach is different from the original methodology only in steps 1 and 4. The savings in computational time from step 1 is much more significant than that obtained from step 4. In step 1 of the original methodology, we sequentially solve for 100 iterations of the planning model using a single thread, for which the total solution time is approximately 10 days. The myopic approach completes step 1 in a little over 4 hours. As regards step 4, the savings are more modest, though significant. For each of the fleet sizes, we compute 20 iterations of the step 4, 10 using the myopic approach and 10 using the original methodology. The box plots in Figure 9a show the reductions in computation time. It can be seen that for 500 SAEVs, the myopic approach obtains the solution in about 2 minutes, whereas the original methodology takes about 120 minutes. Hereafter, we assessed the quality of the solution obtained by the myopic approach as shown in Figure 9b. We notice that the myopic approach yields on average an optimality gap of 21.5%, and it does not appear to be influenced by the fleet size.

Using the myopic approach, we examined the impact of the hub capacity on gross profit, SAEV idle time, and unsatisfied demands in the CPS for a 24 hour period. Hub capacities between 50 and 250 for each hub were considered for fleet sizes of 500, 1000, 2000, and 5000. The results are shown in Figure 10. Regarding gross profit, we notice that for fleet size of 500, the gross profit is almost constant. The hub capacity of 50 for a fleet of 500 is already too high and increasing it further has little to no impact on gross profit. The fleet of 1000 vehicles benefits from an increase in hub capacity beyond 50, but its gross profit does not grow much after a hub capacity of 100. For fleet sizes of 2000 and 5000, the gross profit continues to rise as the hub capacity increases. An interesting observation is that for the fleet of 5000, the gross profits are lower than those for the fleet of 2000. This is due to the fact that a fleet size of 5000 is too high for the range of hub capacities (50-250), and hence many of the SAEVs have to park and idle at the hubs and wait for charging facility to become available. While parked, SAEVs pay a parking fee, thus lowering the gross profit. The gross profit from the fleet of 5000 should be higher than the fleet of 2000 for hub capacities beyond 250. As regards idle time of the SAEVs, it becomes smaller as the hub capacity increases, for all fleet sizes. Note that in the myopic approach, SAEVs idle only when there is either no demand for transportation and/or there is no available charging/discharging facility. Since 50 charging stations per hub is large enough, the fleet of 500

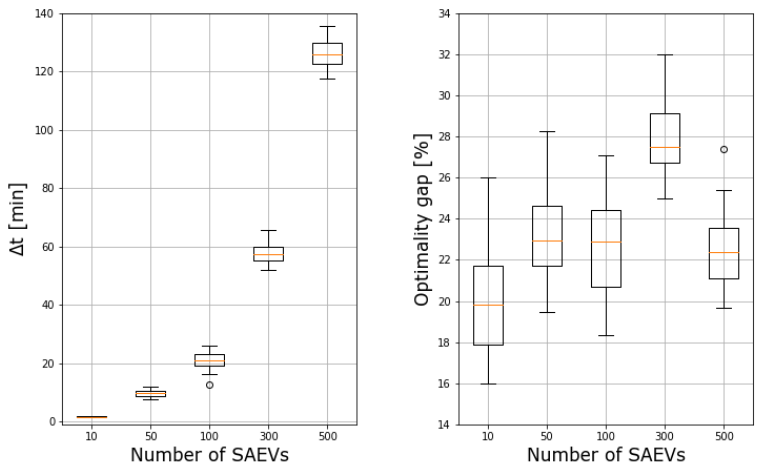

Figure 9: Myopic vs. Optimal solution: time and optimality gap comparison

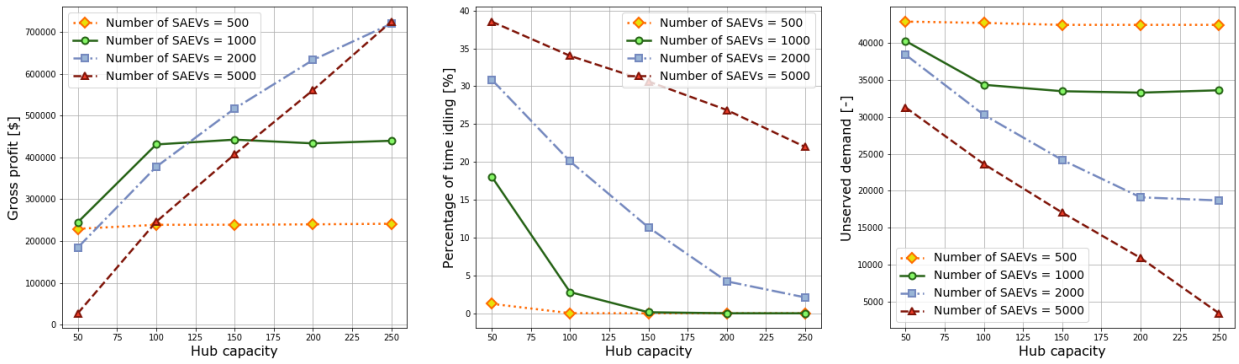

Figure 10: Impact of hub capacity on system performance

has little to no idle time. For a fleet size of 1000, the idle time reaches zero at hub capacity of 150. Fleets of 2000 and 5000 can benefit from hub capacities higher than 250, as the idle time continues to decrease and gross profit continues to increase. Finally, as expected, the unserved passenger demand also decreases as the hub capacity increases. Note that the unserved demand can be reduced only to a point, which depends on the fleet size, by increasing hub capacity. Since the fleet size of 5000 is very large for the given demand, it appears that by increasing hub capacity beyond 250 the unserved demand may be driven to zero.

8 Concluding remarks

Various alliances of technology and manufacturing companies are earnestly developing and testing autonomous electric vehicles capable of navigating busy streets in major cities. These developments are likely to bring a major transformation in which shared autonomous electric vehicles (SAEVs) will replace a significant number of the human driven automobiles used by the ride sharing companies. However, effective switching to fleets of SAEVs will be possible if cyber-physical infrastructure needed for this change are made available in cities

and suburbs. These systems will provide the physical facilities (hubs and the power network infrastructure) for the vehicles to charge and discharge, and also make the real time decisions for the vehicles and the hubs. This paper presents a methodology that yields optimal operational strategies for a fleet of SAEVs and its supporting CPS to maximize gross profit for the system. Recognizing the computational challenges of our methodology, we have also developed a heuristic (myopic) version of the methodology. The myopic methodology is capable of obtaining near optimal operating strategies for ride sharing services with large fleets of SAEVs. Our methodology is novel as it incorporates power network considerations in SAEV fleet operation planning. Existing papers addressing transportation with autonomous electric vehicles focus mostly on the transportation aspects, while making simplifying assumptions for power related issues. Power systems considerations including the use of an alternating current optimal power flow (ACOPF) model, power purchase by the hubs in the day-ahead market, real time price spikes, arbitrage with battery banks, and solar generation have not been presented to the SAEV literature before. Our numerical study shows that ACOPF-guided SAEV fleet planning can yield between \$2000–\$3000 in savings per day (near a million dollars per year) for a service provider with a relatively small fleet size of 500 SAEVs under the given conditions of our study. Our study also unravels an interesting insight about limited potential for energy arbitrage via vehicle-to-grid (V2G) using the SAEV batteries. This is so because in the presence of sufficient transportation demand and a moderate level of real time price spikes, the SAEVs can earn more revenue serving passengers in comparison to engaging in V2G.

Our methodology does not guide on how to select the optimal number of hubs needed for a system as well as how to locate the hubs appropriately within the transportation service network. Also, it did not consider the costs of the vehicles, the hubs (land, building, and charging technology), repair and maintenance, and other statutory needs. Appropriate consideration of the above aspects can yield a more comprehensive methodology for both design as well as operation of a system of SAEVs and the supporting CPS. However, computational complexities associated with obtaining the optimal solution using such a methodology might make its implementation difficult; this is a topic of our future research.

References

Alonso-Mora, J., Wallar, A. & Rus, D. (2017), Predictive routing for autonomous mobility-on-demand systems with ride-sharing, *in* '2017 IEEE/RSJ International Conference on Intelligent Robots and Systems (IROS)', IEEE, pp. 3583–3590.

Bell, M. G. (1991), 'The estimation of origin-destination matrices by constrained generalised least squares', *Transportation Research Part B: Methodological* **25**(1), 13–22.

Bertsimas, D. & Sim, M. (2004), 'The price of robustness', *Operations research* **52**(1), 35–53.

Chen, T. D., Kockelman, K. M. & Hanna, J. P. (2016), 'Operations of a shared, autonomous, electric vehicle fleet: Implications of vehicle & charging infrastructure decisions', *Transportation Research Part A: Policy and Practice* **94**, 243–254.

Das, D. & Wollenberg, B. F. (2005), 'Risk assessment of generators bidding in day-ahead market', *IEEE Transactions on power systems* **20**(1), 416–424.

Farhan, J. & Chen, T. D. (2018), 'Impact of ridesharing on operational efficiency of shared autonomous electric vehicle fleet', *Transportation Research Part C: Emerging Technologies* **93**, 310–321.

Growe-Kuska, N., Heitsch, H. & Romisch, W. (2003), Scenario reduction and scenario tree construction for power management problems, *in* 'Power tech conference proceedings, 2003 IEEE Bologna', Vol. 3, IEEE, pp. 7–pp.

Iacobucci, R., McLellan, B. & Tezuka, T. (2018*a*), Model predictive control of a shared autonomous electric vehicles system with charge scheduling and electricity price response, *in* '2018 3rd IEEE International Conference on Intelligent Transportation Engineering (ICITE)', IEEE, pp. 110–114.

Iacobucci, R., McLellan, B. & Tezuka, T. (2018*b*), 'The synergies of shared autonomous electric vehicles with renewable energy in a virtual power plant and microgrid', *Energies* **11**(8), 2016.

Iacobucci, R., McLellan, B. & Tezuka, T. (2019), 'Optimization of shared autonomous electric vehicles operations with charge scheduling and vehicle-to-grid', *Transportation Research Part C: Emerging Technologies* **100**, 34–52.

Inman, R. H., Pedro, H. T. & Coimbra, C. F. (2013), 'Solar forecasting methods for renewable energy integration', *Progress in energy and combustion science* **39**(6), 535–576.

Jabr, R. A. (2006), 'Radial distribution load flow using conic programming', *IEEE transactions on power systems* **21**(3), 1458–1459.

Jabr, R. A. (2008), 'Optimal power flow using an extended conic quadratic formulation', *IEEE transactions on power systems* **23**(3), 1000–1008.

Kang, N., Feinberg, F. M. & Papalambros, P. Y. (2017), 'Autonomous electric vehicle sharing system design', *Journal of Mechanical Design* **139**(1), 011402.

Lam, A. Y., James, J., Hou, Y. & Li, V. O. (2018), 'Coordinated autonomous vehicle parking for vehicle-to-grid services: Formulation and distributed algorithm', *IEEE Transactions on Smart Grid* **9**(5), 4356–4366.

Li, F. & Bo, R. (2010), Small test systems for power system economic studies, *in* 'IEEE PES general meeting', IEEE, pp. 1–4.

Melendez, K. A., Subramanian, V., Das, T. K. & Kwon, C. (2019), 'Empowering end-use consumers of electricity to aggregate for demand-side participation', *Applied Energy* **248**, 372–382.

Miao, H., Jia, H., Li, J. & Qiu, T. Z. (2019), 'Autonomous connected electric vehicle (acev)-based car-sharing system modeling and optimal planning: A unified two-stage multi-objective optimization methodology', *Energy* **169**, 797–818.

Sedighizadeh, M., Mohammadpour, A. & Alavi, S. M. M. (2019), 'A daytime optimal stochastic energy management for ev commercial parking lots by using approximate dynamic programming and hybrid big bang big crunch algorithm', *Sustainable cities and society* **45**, 486–498.

Smith, C. A. & Corripio, A. B. (1997), *Principles and practice of automatic process control*, Vol. 2, Wiley New York.

Subramanian, V. & Das, T. K. (2019), 'A two-layer model for dynamic pricing of electricity and optimal charging of electric vehicles under price spikes', *Energy* **167**, 1266–1277.

Turan, M. T., Ates, Y., Erdinc, O., Gokalp, E. & Catalão, J. P. (2019), 'Effect of electric vehicle parking lots equipped with roof mounted photovoltaic panels on the distribution network', *International Journal of Electrical Power & Energy Systems* **109**, 283–289.

Uber (2020), 'Uber movement', `https://movement.uber.com/?lang=en-US`. accessed: February 23, 2020.

Verter, V. (2011), Uncapacitated and capacitated facility location problems, *in* 'Foundations of location analysis', Springer, pp. 25–37.

Yao, L., Lim, W. H. & Tsai, T. S. (2017), 'A real-time charging scheme for demand response in electric vehicle parking station', *IEEE Transactions on Smart Grid* **8**(1), 52–62.

Zhang, R., Rossi, F. & Pavone, M. (2016), Model predictive control of autonomous mobility-on-demand systems, *in* '2016 IEEE International Conference on Robotics and Automation (ICRA)', IEEE, pp. 1382–1389.

Zhou, X., Qin, X. & Mahmassani, H. S. (2003), 'Dynamic origin-destination demand estimation with multiday link traffic counts for planning applications', *Transportation Research Record* **1831**(1), 30–38.

Appendix A Alternative current optimal power flow (ACOPF)

It has been shown that the conventional non-linear load flow equations for both radial (Jabr 2006) and meshed networks (Jabr 2008) can be transformed into a second order cone program (SOCP). In this section, we present a modified version of such formulations.

A.1 ACOPF model notations

Sets

- $\mathcal{G}$: Set of all generators in the network
- $\mathcal{N}$: Set of all buses in the network
- $\mathcal{G}_i$: Subset of generators that are connected to bus $i \in \mathcal{N}$
- $\mathcal{N}_i$: Subset of buses that are directly linked to bus $i \in \mathcal{N}$
- $\mathcal{T}$: Set of all time periods
- $\mathcal{L}$: Set of all lines in the network

Parameters

- P^L_{it}: Active power load at bus $i \in \mathcal{N}$ at time $t \in \mathcal{T}$
- Q^L_{it}: Reactive power load at bus $i \in \mathcal{N}$ at time $t \in \mathcal{T}$
- G_{ij}: Conductance of line $ij \in \mathcal{L}$
- B_{ij}: Susceptance of line $ij \in \mathcal{L}$
- F^+_{ij}, F^-_{ij}: Real and reactive power capacity of line $ij \in \mathcal{L}$, respectively

- $\underline{P_g}$, $\overline{P_g}$: Lower and upper bound, respectively, of real power supply by generator $g \in \mathcal{G}$
- $\underline{Q_g}$, $\overline{Q_g}$: Lower and upper bound, respectively, of reactive power supply by generator $g \in \mathcal{G}$
- $\underline{V_i}$, $\overline{V_i}$: Voltage lower and upper bound, respectively, at node $i \in \mathcal{N}$

Decision variables

- p_{gt}: Real power dispatch from generator $g \in \mathcal{G}$ at time $t \in \mathcal{T}$
- q_{gt}: Reactive power dispatch form generator $g \in \mathcal{G}$ at time $t \in \mathcal{T}$

Other variables

- p_{ijt}: Real power flow from bus $i \in \mathcal{N}$ to node $j \in \mathcal{N}$ at time $t \in \mathcal{T}$
- q_{ijt}: Reactive power flow from bus $i \in \mathcal{N}$ to node $j \in \mathcal{N}$ at time $t \in \mathcal{T}$
- u_{it}: Transformed voltage at bus $i \in \mathcal{N}$ and time $t \in \mathcal{T}$; $u_{it} = \frac{V_{it}^2}{\sqrt{2}}$, where V_{it} is the actual voltage at node $i \in \mathcal{N}$ and time $t \in \mathcal{T}$ and it can be calculated after the optimization model is solved
- r_{ijt}: Intermediate variable; $r_{ijt} = V_{it}V_{jt}\cos(\theta_i - \theta_j)$, where θ_i and θ_j are the voltage angles at buses $i \in \mathcal{N}$ and $j \in \mathcal{N}$, respectively
- $\bar{r}_{ijt}$: Intermediate variable; $\bar{r}_{ijt} = V_{it}V_{jt}\sin(\theta_i - \theta_j)$

A.2 ACOPF model formulation

The SOCP formulation of the traditional non-linear ACOPF problem is presented below.

$$\min \quad \sum_{t\in\mathcal{T}}\sum_{g\in\mathcal{G}} C_g(p_{gt}) \tag{43}$$

$$\text{s.t.,} \quad \sum_{g\in\mathcal{G}_i} p_{gt} - \sum_{j\in\mathcal{N}_i} p_{ijt} = P_{it}^L \qquad \forall i \in \mathcal{N}, t \in \mathcal{T} \tag{44}$$

$$\sum_{g\in\mathcal{G}_i} q_{gt} - \sum_{i\in\mathcal{N}_i} q_{ijt} = Q_{it}^L \qquad \forall i \in \mathcal{N}, t \in \mathcal{T} \tag{45}$$

$$p_{ijt} = \sqrt{2}G_{ij}u_{it} - G_{ij}r_{ijt} + B_{ij}\bar{r}_{ijt} \qquad \forall ij \in \mathcal{L}, t \in \mathcal{T} \tag{46}$$

$$q_{ijt} = \sqrt{2}B_{ij}u_{it} - B_{ij}r_{ijt} - G_{ij}\bar{r}_{ijt} \qquad \forall ij \in \mathcal{L}, t \in \mathcal{T} \tag{47}$$

$$-F_{ij}^+ \le p_{ijt} \le F_{ij}^+ \qquad \forall ij \in \mathcal{L}, t \in \mathcal{T} \tag{48}$$

$$-F_{ij}^- \le q_{ijt} \le F_{ij}^- \qquad \forall ij \in \mathcal{L}, t \in \mathcal{T} \tag{49}$$

$$\underline{P_g} \le p_{gt} \le \overline{P_g} \qquad \forall g \in \mathcal{G}, t \in \mathcal{T} \tag{50}$$

$$\underline{Q_g} \le q_{gt} \le \overline{Q_g} \qquad \forall g \in \mathcal{G}, t \in \mathcal{T} \tag{51}$$

$$\frac{1}{\sqrt{2}}\underline{V_i}^2 \le u_{it} \le \frac{1}{\sqrt{2}}\overline{V_i}^2 \qquad \forall i \in \mathcal{N}, t \in \mathcal{T} \tag{52}$$

$$r_{ijt}^2 + \bar{r}_{ijt}^2 \le 2u_{it}u_{jt} \qquad \forall ij \in \mathcal{L}, t \in \mathcal{T} \tag{53}$$

$$r_{ijt} = r_{jit} \qquad \forall\, ij \in \mathcal{L} \tag{54}$$

$$\bar{r}_{ijt} = -\bar{r}_{jit} \qquad \forall\, ij \in \mathcal{L} \tag{55}$$

In the objective function (43), $C_g(\cdot)$ denotes the cost function of generator g. Hence, the above formulation minimizes the total electricity cost of the network over all time periods. Real and reactive power balance

at node i and time period t are considered by equations (44) and (45), respectively. Equations (46) and (47) are the real and reactive power flows, respectively, from node i to node j at time period t. Real and reactive line flow capacities of arc ij are given by equations (48) and (49). Equation (50) and (51) bound the generators real and reactive power outputs, respectively. Equation (52) bounds the voltage of each node of the network. Equation (53) is a conic constraint to account for the relation between power flow components and the voltage at each node. Finally, Equations (54) and (55) consider the relation between the power flowing from node i to j and the power flowing from j to i. Also, the voltage at node 1 (substation node) is considered to be known. Hence, we can write that $u_{1t} = \frac{V_1^2}{\sqrt{2}}\ \forall t \in \mathcal{T}$. The above formulation is a SOCP since any constraint of the form $\{u, v, w \geq 0 : u \leq \sqrt{vw}\}$ is equivalent to $\{u, v, w \geq 0 : \sqrt{u^2 + (\frac{v-w}{2})^2}\} \leq \frac{v+w}{2}\}$.

Appendix B Robustification of the operational model

B.1 Robust optimization

Robust optimization is an approach to solve linear optimization problems for which one or more coefficients are random variables. This approach obtains suboptimal solutions considering the mean values of the random variables but ensures feasibility and near optimality when the coefficients deviate from the mean. In what follows, before robustifying our model (35), we exemplify the process by developing a robust reformulation of a generic linear programming model.

Consider the following linear optimization problem.

$$\begin{aligned} \max \quad & c^\intercal x \\ \text{s.t.}, \quad & Ax \leq b, \\ & x \in \mathcal{X}, \end{aligned} \tag{56}$$

where A is an $m \times n$ matrix, x is an $n \times 1$ vector (decision variables), $c^\intercal$ is a $1 \times n$ vector, and b is a $m \times 1$ vector. Without loss of generality, it is considered that the randomness only affects the elements in matrix A, since we can always re-write the problem as:

$$\begin{aligned} \max \quad & z \\ \text{s.t.}, \quad & z - c^\intercal x \leq 0, \\ & Ax - bY \leq 0, \\ & x \in \mathcal{X}, \\ & Y = 1. \end{aligned} \tag{57}$$

Consider a particular row i of the matrix A and let $\mathcal{J}_i$ represent the set of coefficients in row i that are subject to uncertainty. Also, it is considered that the probability distribution of each component $a_{ij}, j \in \mathcal{J}_i$ is unknown, but the values in which a_{ij} ranges are known and defined by $[\bar{a}_{ij} - \hat{a}_{ij}, \bar{a}_{ij} + \hat{a}_{ij}]$, where $\bar{a}_{ij}$ is the best estimate of a_{ij}, and $\hat{a}_{ij}$ is maximum feasible deviation from $\bar{a}_{ij}$. Bertsimas & Sim (2004) proved that the robust counterpart of a linear problem with the form of (56) can be also formulated by introducing a set of non-negative variables (y_j, p_{ij}, and z_i) and a parameter Γ_i that takes values in the interval $[0, |\mathcal{J}_i|]$. The role of Γ_i is to adjust the robustness of the proposed method against the level of conservatism of the solution (Bertsimas & Sim 2004). Then, the robust reformulation of (56) is given by:

$$
\begin{aligned}
\max \quad & c^{\intercal} x \\
\text{s.t.}, \quad & \sum_j \bar{a}_{ij} x_j + z_i \Gamma_i + \sum_{j \in \mathcal{J}_i} p_{ij} \leq b_i \qquad \forall i, \\
& z_i + p_{ij} \geq \hat{a}_{ij} y_j \qquad \forall i, j \in \mathcal{J}_i, \\
& -y_j \leq x_j \leq y_j \qquad \forall j, \\
& x_j \in \mathcal{X} \qquad \forall j, \\
& p_{ij} \geq 0 \qquad \forall i, j \in \mathcal{J}_i, \\
& y_j \geq 0 \qquad \forall j, \\
& z_i \geq 0 \qquad \forall i.
\end{aligned} \tag{58}
$$

The solution of (58) is robust against the expected disturbances in the parameters of the model.

B.2 Robust counterpart of the operational model

In this subsection, we present the robust versions of the constraints with uncertain parameters, namely, constraints (1), (19), (20), (30), (31), and (34). Recall that the state of the system is completely known at the current time period τ, and hence, the robust constraints are only included for time periods $\tau + 1$ and onward. Then, we can write the robust re-formulations following Bertsimas & Sim (2004).

- Robust counterpart of constraint (1):

$$d_{ij,\tau+1} = \beta d_{ij\tau} + \gamma_{ij\tau} - \sum_{b \in \mathcal{B}} x^b_{ij\tau} - b_{ijt} \qquad \forall (i,j) \in \overline{\mathcal{N}} \tag{59}$$

$$d_{ij,t+1} = \beta d_{ijt} + \bar{\gamma}_{ijt} Y^{\gamma}_{ijt} - \sum_{b \in \mathcal{B}} x^b_{ijt} - b_{ijt} - z^{\gamma}_{ijt} \Gamma^{\gamma}_{ijt} - q^{\gamma}_{ijt} \; \forall (i,j) \in \overline{\mathcal{N}}, t \in \{\tau+1, \cdots, |\overline{\mathcal{T}}|\} \tag{60}$$

$$z^{\gamma}_{ijt} + q^{\gamma}_{ijt} \geq \hat{\gamma}_{ijt} y^{\gamma}_{ijt} \; \forall (i,j) \in \overline{\mathcal{N}}, t \in \{\tau+1, \cdots, |\overline{\mathcal{T}}|\} \tag{61}$$

$$-y^{\gamma}_{ijt} \leq Y^{\gamma}_{ijt} \leq y^{\gamma}_{ijt} \qquad \forall (i,j) \in \overline{\mathcal{N}}, t \in \{\tau+1, \cdots, |\overline{\mathcal{T}}|\} \tag{62}$$

$$Y^{\gamma}_{ijt} = 1 \qquad \forall (i,j) \in \overline{\mathcal{N}}, t \in \{\tau+1, \cdots, |\overline{\mathcal{T}}|\} \tag{63}$$

- Robust counterpart of constraint (19):

$$\sum_{b \in \mathcal{B}} f^b_{h\tau} + f^+_{h\tau} + f^-_{h\tau} = F_{ht} \qquad \forall h \in \mathcal{H} \tag{64}$$

$$\sum_{b \in \mathcal{B}} f^b_{ht} + f^+_{ht} + f^-_{ht} = \overline{F}_{ht} Y^F_{ht} - z^{\mathrm{F}}_{ht} \Gamma^F_{ht} - q^F_{ht} \qquad \forall h \in \mathcal{H}, t \in \{\tau+1, \cdots, |\overline{\mathcal{T}}|\} \tag{65}$$

$$z^F_{ht} + q^F_{ht} \geq \hat{F}_{ht} y^F_{ht} \qquad \forall h \in \mathcal{H}, t \in \{\tau+1, \cdots, |\overline{\mathcal{T}}|\} \tag{66}$$

$$-y^F_{ht} \leq Y^F_{ht} \leq y^F_{ht} \forall h \in \mathcal{H}, t \in \{\tau+1, \cdots, |\overline{\mathcal{T}}|\} \tag{67}$$

$$Y^F_{ht} = 1, \qquad \forall h \in \mathcal{H}, t \in \{\tau+1, \cdots, |\overline{\mathcal{T}}|\} \tag{68}$$

- Robust counterpart of constraint (20):

$$w^v_{h,\tau+1} \leq W^v_{h\tau} \qquad \forall h \in \mathcal{H}, v \in \{1, \cdots, V\} \tag{69}$$

$$w^v_{h,t+1} \leq \overline{W}^v_{ht} Y^{v,\mathrm{EV}}_{ht} - z^{v,\mathrm{EV}}_{ht} \Gamma^{v,\mathrm{EV}}_{ht} - q^{v,\mathrm{EV}}_{ht} \; \forall h \in \mathcal{H}, t \in \{\tau+1, \cdots, |\overline{\mathcal{T}}|\}, v \in \{1, \cdots, V\} \tag{70}$$

$$z^{v,\mathrm{EV}}_{ht} + q^{v,\mathrm{EV}}_{ht} \geq \hat{W}^v_{ht} y^{v,\mathrm{EV}}_{ht} \; \forall h \in \mathcal{H}, t \in \{\tau+1, \cdots, |\overline{\mathcal{T}}|\}, v \in \{1, \cdots, V\} \tag{71}$$

$$-y_{ht}^{v,\mathrm{EV}} \leq Y_{ht}^{v,\mathrm{EV}} \leq y_{ht}^{v,\mathrm{EV}} \; \forall h \in \mathcal{H}, t \in \{\tau+1, \cdots, |\overline{\mathcal{T}}|\}, v \in \{1, \cdots, V\} \tag{72}$$

$$Y_{ht}^{v,\mathrm{EV}} = 1 \; \forall h \in \mathcal{H}, t \in \{\tau+1, \cdots, |\overline{\mathcal{T}}|\}, v \in \{1, \cdots, V\} \tag{73}$$

- Robust counterpart of constraint (30):

$$a^{\mathrm{RT}} = \sum_{h \in \mathcal{H}} \pi_{h\tau}^{\mathrm{RT}} l_{h\tau}^{\mathrm{RT}} + \sum_{h \in \mathcal{H}} \sum_{t=\tau+1}^{|\overline{\mathcal{T}}|} \bar{\pi}_{ht}^{\mathrm{RT}} l_{ht}^{\mathrm{RT}} - z_{\mathrm{RT}} \Gamma_{\mathrm{RT}} - \sum_{h \in \mathcal{H}} \sum_{t=\tau+1}^{|\overline{\mathcal{T}}|} q_{ht}^{\mathrm{RT}} \tag{74}$$

$$z_{\mathrm{RT}} + q_{ht}^{\mathrm{RT}} \geq \hat{\pi}_{ht}^{\mathrm{RT}} y_{ht}^{\mathrm{RT}} \qquad \forall h \in \mathcal{H}, t \in \{\tau+1, \cdots, |\overline{\mathcal{T}}|\} \tag{75}$$

$$-y_{ht}^{\mathrm{RT}} \leq l_{ht}^{\mathrm{RT}} \leq y_{ht}^{\mathrm{RT}} \qquad \forall h \in \mathcal{H}, t \in \{\tau+1, \cdots, |\overline{\mathcal{T}}|\} \tag{76}$$

- Robust counterpart of constraint (31):

$$a_b^{\mathrm{RT}} = \sum_{h \in \mathcal{H}} \pi_{h\tau}^{\mathrm{RT}} l_{h\tau}^{b,\mathrm{RT}} + \sum_{h \in \mathcal{H}} \sum_{t=\tau+1}^{|\overline{\mathcal{T}}|} \bar{\pi}_{ht}^{\mathrm{RT}} l_{ht}^{b,\mathrm{RT}} - z_{b,\mathrm{RT}} \Gamma_{b,\mathrm{RT}} - \sum_{h \in \mathcal{H}} \sum_{t=\tau+1}^{|\overline{\mathcal{T}}|} q_{ht}^{b,\mathrm{RT}} \; \forall b \in \mathcal{B} \tag{77}$$

$$z_{b,\mathrm{RT}} + q_{ht}^{b,\mathrm{RT}} \geq \hat{\pi}_{ht}^{\mathrm{RT}} y_{ht}^{b,\mathrm{RT}} \qquad \forall b \in \mathcal{B}, h \in \mathcal{H}, t \in \{\tau+1, \cdots, |\overline{\mathcal{T}}|\} \tag{78}$$

$$-y_{ht}^{b,\mathrm{RT}} \leq l_{ht}^{b,\mathrm{RT}} \leq y_{ht}^{b,\mathrm{RT}} \qquad \forall b \in \mathcal{B}, h \in \mathcal{H}, t \in \{\tau+1, \cdots, |\overline{\mathcal{T}}|\} \tag{79}$$

- Robust counterpart of constraint (34):

$$a^{\mathrm{RT}} = \sum_{h \in \mathcal{H}} (\pi_{ht}^{\mathrm{RT}} - \delta^{\mathrm{RT}}) p_{ht}^{\mathrm{RT}-} + \sum_{h \in \mathcal{H}} \sum_{t=\tau+1}^{|\overline{\mathcal{T}}|} (\hat{\pi}_{ht}^{\mathrm{RT}} - \delta^{\mathrm{RT}}) p_{ht}^{\mathrm{RT}-} - z_{\mathrm{DA}} \Gamma_{\mathrm{DA}} - \sum_{h \in \mathcal{H}} \sum_{t=\tau+1}^{|\overline{\mathcal{T}}|} q_{ht}^{\mathrm{DA}} \tag{80}$$

$$z_{\mathrm{DA}} + q_{ht}^{\mathrm{DA}} \geq \hat{\pi}_{ht}^{\mathrm{RT}} y_{ht}^{\mathrm{DA}} \qquad \forall h \in \mathcal{H}, t \in \{\tau+1, \cdots, |\overline{\mathcal{T}}|\} \tag{81}$$

$$-y_{ht}^{\mathrm{DA}} \leq p_{ht}^{\mathrm{RT}-} \leq y_{ht}^{\mathrm{DA}} \qquad \forall h \in \mathcal{H}, t \in \{\tau+1, \cdots, |\overline{\mathcal{T}}|\} \tag{82}$$

All the new variables introduced in the above robust constraints satisfy the conditions established in subsection B.1. Also note that, $\pi_{h\tau}^{\mathrm{RT}}$, $F_{h\tau}$, W_{ht}^{v}, and $\gamma_{ij\tau}$ are known, while $\bar{\pi}_{ht}^{\mathrm{RT}}$, $\overline{F}_{ht}$, $\overline{W}_{ht}^{v}$, and $\bar{\gamma}_{ijt}$ $\forall t \in \{\tau+1, \cdots, |\overline{\mathcal{T}}|\}$ are the best estimates of these parameters for the remaining time periods. We estimate the RT prices (with spikes) as $\bar{\pi}_{ht}^{\mathrm{RT}} = \pi_{ht}^{\mathrm{DA}}(1+\epsilon)$. There are many techniques available to estimate the available solar power $\overline{F}_{ht}$. In Inman et al. (2013), the authors review the theory behind these forecasting methodologies, and present a number of successful applications of solar forecasting methods for both the solar resource and the power output of solar plants. Estimating origin-destination (O-D) matrices is also a widely studied area. A mayor reference in this area is Bell (1991). More recently, an O-D prediction algorithm for autonomous mobility-on-demand systems with ride-sharing was proposed in Alonso-Mora et al. (2017). The authors used historical data to compute a probability distribution of the future demand. Thereafter, they incorporate samples from the above probability distribution into a decoupled vehicle routing and passenger assignment method. The values of $\overline{W}_{ht}^{v}$ and $\bar{\gamma}_{ijt}$ are chosen equal to the mean value of the fitted probability distributions. Finally, the values of $\hat{\pi}_{ht}^{\mathrm{RT}}$, $\hat{F}_{ht}$, $\hat{W}_{ht}^{v}$, $\hat{\nu}_{ht}$, and $\hat{\gamma}_{ijt}$ $\forall t \in \{\tau+1, \cdots, |\overline{\mathcal{T}}|\}$ are chosen such that the maximum deviation from the best estimate matches the confidence interval of the selected forecast method.